This is a post-print of an article that was accepted for publication in Basin Research on January 6th, 2023.

The present document is the revised manuscript submitted to Basin Research on December 10th, 2022. An earlier version of the manuscript was submitted to Basin Research on December 23rd, 2021.

Title:

The evolution of catchment-depositional system relationships on the dip slopes of intra-rift basement highs: an example from the Frøya High, Mid-Norwegian Rifted Margin

Authors:

Gijs A. Henstra*, Aker BP, Oksenøyveien 10, 1366 Lysaker, Norway

Timothy M. Cullen, Department of Earth Science, University of Bergen, PO Box 7800, 5020 Bergen, Norway

Robert L. Gawthorpe, Department of Earth Science, University of Bergen, PO Box 7800, 5020 Bergen, Norway

Jhon M. Munoz-Barrera, Department of Earth Science, University of Bergen, PO Box 7800, 5020 Bergen, Norway

Martin Muravchik, Department of Earth Science, University of Bergen, PO Box 7800, 5020 Bergen, Norway

Atle Rotevatn, Department of Earth Science, University of Bergen, PO Box 7800, 5020 Bergen, Norway

\) corresponding author; gijshenstra@gmail.com

The evolution of catchment-depositional system relationships on the dip slopes of intra-rift basement highs: an example from the Frøya High, Mid-Norwegian Rifted Margin

Gijs A. Henstra[1,2], Timothy M. Cullen [1], Robert L. Gawthorpe[1], Jhon M. Munoz-Barrera[1], Martin Muravchik[1], Atle Rotevatn[1].

1. *Department of Earth Science, University of Bergen, Bergen, Norway*
2. *Aker BP, Oksenøyveien 10, 1366 Lysaker, Norway*

Abstract

Basement highs form one of many potential sediment source areas during the evolution of continental rifts and rifted margins and add to the topographic complexity typical of active rifts. Footwall basement highs acting as a source area to sedimentary systems in the hangingwall of major faults has been documented in many systems worldwide. However, the back-tilted footwall dip slopes of such highs have received comparatively little attention. Here we investigate a subsurface case study from the Norwegian continental shelf, where catchments and shallow marine syn-rift sedimentary systems on a dip slope are preserved due to early transgression of an intra-rift high. At the onset of Late Jurassic rifting, the Frøya High emerged as a prominent, N-S trending, 25 km wide basement high tilted towards the east in response to several kilometers of displacement along the Klakk Fault Complex, a major normal fault zone at the Frøya High's western edge. Using well-calibrated 3D seismic reflection data, we observe a series of conspicuous Upper Jurassic wedges along the eastern edge of the Frøya High along the margin of the Froan Basin. Internally, these wedges show sigmoidal geometries marking top- and foresets of clinoform packages with a maximum thickness of *ca*. 200 meters with foresets between 30 – 200 m high, dipping *ca*. 10 degrees towards the east, south east and north east. We interpret these wedges to represent a series of eastward prograding deltas positioned along a constructional shoreline, connected to E-W trending valleys and river catchments updip. The deltas show strong progradation, interpreted to reflect the impact of continued uplift of their catchments. prior to abrupt termination of sediment supply from drainage capture by footwall scarp drainages. The presence of a connected, largely constructional shoreline has implications for Late Jurassic sediment distribution around the Frøya High, providing primary sedimentary input for longshore driven sedimentary systems in the Draugen Ridge to the north. Comparisons with other syn-rift dip slope systems highlights a broadly similar evolution but shows a distinct lack of the protracted backstepping observed in other dip slope systems. We postulate that different structural configurations of dip slope systems, being footwall uplift,

or hangingwall subsidence driven, may drive the strongly progradational character of the deltaic systems on the Frøya High. The Frøya High example highlights the need to constrain primary sediment input points to aid interpretation of volumetrically significant, but short-lived and subtle depositional systems, especially within complex, tectonically active settings.

1 Introduction

The evolution of rift basins promotes a wide variety of sediment routing and depositional systems which can vary considerably over relatively short temporal and spatial scales (e.g., Gawthorpe et al., 1994; Ravnås & Steel, 1998; Gawthorpe & Leeder, 2000; Nøttvedt et al., 2000; Barrett et al., 2019). High rates and magnitudes of subsidence in the hangingwall of active structures produce the greatest areas of accommodation, with many studies focussing on the delivery of sediment from drainage catchments on nearby footwall crests (e.g., Bilal et al., 2018; Barrett et al., 2021). However, uplift and rotation of the back-tilted footwall dip slope also offers accommodation for sedimentary systems fed by drainage directed away from the footwall crest. (Ravnås & Steel., 1998; Gawthorpe & Leeder, 2000; Muravchik et al., 2018; Smyrak-Sikora et al., 2018; 2021; Rapozo et al., 2021). The tectono-sedimentary setting of dip slopes developed along the footwall of major faults is considerably different to that of immediate hangingwall systems such as fault-scarp degradation related fans, or rift-margin deltas. Lower gradients and subsidence rates, of backtilted slopes in the footwall of major normal faults, leads to a greatly enhanced sensitivity to eustatic changes across broader, shallower landscapes compared to hangingwall depocentres and commonly host shoreline depositional systems (Gawthorpe et al., 1994; Bell et al., 2018; Fernàndez-Blanco et al., 2020; Smyrak-Sikora et al., 2021). However, the controls upon the spatial variability in depositional environment and resultant stratigraphic architecture of dip slope shoreline systems in rift settings remains comparatively unclear, especially those flanking large intra-rift basement highs (Nøttvedt et al., 2000; Muravchik et al., 2018). With the exception of few localised outcrop (Jackson et al., 2005; Muravchik et al., 2018; Smyrak-Sikora et al., 2021) and subsurface examples (Ravnås & Steel., 1998; Nøttvedt et al., 2000; Chiarella et al., 2020), there are few studies which address the scales, along-strike variability and potential controls on such syn-rift depositional systems.

Offshore Mid-Norway, at the necking domain of the Norwegian rifted margin, the Frøya High hosts a number of fringing syn-rift depositional systems, formed on the footwall dip slope of a major active rift margin bound by the Klakk and Vingleia fault complexes during the Late Jurassic and Early Cretaceous (Figure 1; Blystad et al., 1995; Bell et al., 2014; Elliott et al., 2015; Muñoz-Barrera et al., 2020; Jones et al., 2020). Except for stratigraphy at the northern end of the Frøya High, near the Draugen ridge (Chiarella et al., 2021), syn-rift sediment routing and depositional systems on the eastern flank of the Frøya High have received little attention. The eastern flank of the Frøya High allows for a coherent investigation into the link between sediment source area and down-dip deposition, partly due to partial preservation of drainage catchments on the Frøya High following a prolonged period of flooding and burial of the Frøya High at the end of the Jurassic (Jones et al., 2020). Excellent 3D seismic data coverage and recent exploration drilling in 2022 has allowed for re-evaluation of stratigraphic relationships between the Frøya High and basinal areas with improved constraints through newly acquired biostratigraphic, wireline and sidewall core samples within the Upper Jurassic, Viking Group stratigraphy. Here, we integrate this seismic and well data to investigate syn-rift sedimentation along a footwall dip slope of a major rift-margin normal fault, the Klakk Fault Complex (Figure 1). Biostratigraphically constrained deposits and surfaces permit the mapping and characterisation of three-dimensional variability of syn--rift drainage catchments in the footwall of the Klakk Fault Complex and dip slopethe associated dip slope depositional systems at the southern and central part of the Frøya High. Finally, integration and comparison of observations from the Frøya High with other dip slopedip slope systems from other rift basins demonstrate the variability and role of structural setting in determining the architecture of dip slope sedmentary systems.

2 Geological setting

2.1 Major tectonic elements and structural evolution of the Frøya High

The Frøya High is situated on the Mid-Norwegian passive margin, between 63°N-64°30'N and 6°30'E-7°20'E (Figure 1) and comprises a granitic basement which delineates a strong positive magnetic and gravity anomaly (Blystad et al., 1995; Olesen et al., 2010; Muñoz-Barrera et al., 2020). It is bounded to the west by the Klakk Fault Complex (KFC) and is located in the necking domain between the hyperextended Møre and Rås Basins (distal domain) and the Trøndelag Platform (proximal domain; Osmundsen and Ebbing, 2008; Mjelde et al., 2009). At the southern part of the Frøya High, the KFC is defined by a 10 – 15 km wide, broad, west-dipping escarpment (Figure 1). The KFC offsets the basement by more than 6 km (Blystad et al., 1995) and reaches the base of the lower crust (Osmundsen & Péron-Pinvidic, 2018; Muñoz-Barrera et al., 2020). The Rås Basin, in the immediate hangingwall of the KFC, has a broadly synformal geometry filled with a ~6-7 km thick Mesozoic-Cenozoic basin fill (Blystad et al., 1995; Muñoz-Barrera et al., 2022).

East of the Frøya High lies the southern tip of the 50 km wide Froan Basin that extends for 250 km north along the Trøndelag Platform (Blystad et al., 1995). The Froan Basin is underlain by thick continental crust and contains a Palaeozoic to Cenozoic sedimentary successions. Unlike the western, fault-controlled margin of the Frøya High, the south-eastern margin of the Frøya High passes into the Froan Basin across a gently east-dipping basement-sediment contact cut by several minor, small-displacement normal faults (Figure 1). In the northern part of the Froan Basin this boundary becomes more distinct where the Froan Basin is delimited by a narrow horst between the Vingleia Fault Complex (VFC) and Froan Fault (Figure 1; Wilson et al., 2015; Elliot et al., 2015, 2017; Gernigon et al., 2019; Osmundsen et al., 2021; Bunkholt et al., 2022).

The Mid-Norwegian margin evolved through several rift episodes following Devonian collapse of the Caledonian mountain range (Coward et al., 2003; Bell et al., 2014). A major rift episode occurred during the Late Permian – Early Triassic leading to crustal stretching and the formation of NE-SW-trending rotated fault blocks on the mid-Norwegian margin (Brekke & Riis, 1987; Brekke, 2000; Coward et al., 2003; Halland et al., 2013; Péron-Pinvidic et al., 2013;). During this time, a smaller basin was generated on the Frøya High informally known as the Almond Basin, a 2-5 km wide and 0.5 s TWT thick half graben filled largely with, unconfirmed but likely, Permian to Middle Jurassic stratigraphy (Figure 1; Blystad et al., 1995;). Following a period of relative tectonic quiescence from the Mid-Triassic through to the Early Jurassic, extension resumed within the Middle Jurassic through to the Late Jurassic (Færseth, 1996; Brekke, 2000; Coward et al., 2003; Roberts et al., 2009). During this Middle-Late Jurassic phase, the main tectonic elements such as the Møre Basin, the Frøya High and the Halten Terrace started to form as the rift reached a widely documented 'thinning' phase and deformation became localised (Osmundsen et al., 2002; Péron-Pinvidic et al., 2013; Osmundsen & Péron-Pinvidic, 2018; Muñoz-Barrera et al., 2020; Bunkholt et al., 2022). The Klakk, Vingleia and Bremmstein fault complexes accumulated substantial displacement at this time and became the location of crustal necking leading to uplift of the Frøya High that emerged as a prominent high, during the latter part of the Middle, and throughout the Late Jurassic – Early Cretaceous within a broader seaway encompassing the approximately 250 km wide and 1500 km long Trøndelag Platform separating Norway and Greenland (Figure 1; Coward et al., 2003; Nøttvedt et al., 2008; Osmundsen & Ebbing, 2008; Péron-Pinvidic et al., 2013; Chiarella et al., 2020; Jones et al., 2020; Bunkholt et al., 2022).

The Froan Basin itself was only moderately tectonically active duringthe Late Jurassic – Early Cretaceous rift episode, with a minor component of uplift on its western margin on to the Frøya High in response to uplift in the footwall of the KFC (Blystad et al., 1995). Following the Late Jurassic – Early Cretaceous rift episode, deformation became focused on the distal domain of the Norwegian Margin, west of the Frøya High (Brekke & Riis, 1987; Blystad et al., 1995; Brekke et al., 1999; Osmundsen et al., 2002; Færseth, 2020).

Throughout the Early Cretaceous, the crust underneath the Møre Basin became hyperextended with substantial displacement accumulated on the KFC (Grunnaleite & Gabrielsen, 1995; Péron-Pinvidic et al., 2013; Osmundsen et al., 2016; Muñoz-Barrera et al., 2020, 2021; Bunkholt et al., 2022). During this time, uplift of the Frøya High began to decrease and it ultimately became buried during the Mid-Late Cretaceous (Bell et al., 2014; Bunkholt et al., 2022).

2.2 Stratigraphic framework of the Late Jurassic – Early Cretaceous rift episode: the Viking Group.

Depositional products of the sedimentary systems that were active on the eastern margin of the Frøya High during the Jurassic – Early Cretaceous rift episode are part of the Middle-Upper Jurassic Viking Group (Figure 2). In the study area the Viking Group either directly overlies the Middle Jurassic Fangst Group, Triassic sediments (known as 'Red' and 'Grey' Beds in local stratigraphic terminology (Blystad et al., 1995), or granitic basement (Figure 2b). The oldest formation of the Viking group is the Callovian-Oxfordian Melke Formation that is commonly interpreted to record the transition from pre-rift to rift initiation in the area of the Frøya High (Blystad et al., 1995; Corfield et al., 2001; Jones et al., 2020; Chiarella et al., 2020). The Melke Formation, where present, is overlain by the Spekk or Rogn formations, that have been linked to 'rift-climax' and late rift phases (Jones et al., 2020). The Spekk Formation is largely mud-prone, high in organic content and is widespread on and around the Frøya High (Jones et al., 2020; Muñoz-Barrera et al., 2020, 2022, Bunkholt et al., 2022;). The Rogn Formation is a distinct sand unit that commonly sits stratigraphically within the Spekk Formation on the eastern flank of the Frøya High (Figure 2b,c, Chiarella et al., 2020). The Rogn Formation is typically interpreted to represent Late Jurassic – Early Cretaceous deposits of shoreface to offshore-bar environments

(Jones et al., 2020; Chiarella et al., 2020) in a narrow seaway between footwall block islands and the Late Jurassic coastline of the Norwegian mainland (Chiarella et al., 2020; Bunkholt et al., 2022; Færseth, 2022). The Viking Group is capped by a regional unconformity, commonly referred to as the Base Cretaceous Unconformity (BCU) which is overlain by deposits of the mud-prone Lyr and Lange formations of the Cromer Knoll Group. In most parts of the study area the Cromer Knoll Group onlaps the BCU. However, the BCU can have a conformable appearance picked out by a high amplitude negative reflector (Figure 2a).

3 Data and Methodology

3.1 3.1 Seismic and well data

This study makes use of a reprocessed 3D seismic reflection survey that covers most of the southern part of the Frøya High from the KFC in the west to the Froan Basin in the east (Figure 1a). Seismic data is in normal polarity, displayed in SEG normal convention (downward increase in acoustic impedance = positive amplitude). The wells 6306/6-1 and 6306/9-1 provide tie-points for the key seismic markers: Top basement, Base Viking Group, Top Viking Group (BCU) and base Upper Cretaceous, and Top Cromer Knoll Group (Figure 2a; Table 1)

Well 6306/6-1 is located on the eastern Frøya High and is used to identify the seismic expression of key stratigraphic events within the syn-rift interval (**Figure 1b, Figure 2**). The sonic and density logs of well 6306/6-1 provide a record of acoustic impedance contrasts within the stratigraphic interval of interest andgeneration of a synthetic seismogram that allows the characteristics of the key stratal surfaces to be constrained (**Figure 2 and Table 1**).

Well Top Name	**Amplitude at 6306/6-1**	**Character**	**Variability**
Top Basement	High amplitude, hard-kick (positive acoustic impedance).	Moderate lateral continuity.	Occasionally lower amplitude where basement is overlain by Mesozoic stratigraphy.
Base Viking	Zero-crossing from positive to negative from moderate positive amplitude to large negative amplitude.	Moderate-limited lateral continuity.	Amplitude variability common.
Base Rogn Formation	Zero-crossing from negative to positive from weakly negative or noisy wavelet to high positive amplitude.	Moderate lateral continuity.	Laterally consistent.
Top Rogn Formation	Zero-crossing from moderate negative to high positive amplitude often with merged or weakly separated doublet.	Strong lateral continuity	Laterally consistent.

Top Viking Group/'BCU'	Strong-moderate soft-kick to high negative amplitude.	Strong lateral continuity to surface.	Unconformable and laterally variable amplitude character.
Top Cromer Knoll	Zero-crossing to high positive amplitude peak from low-amplitude noisy data.	Strong lateral continuity	Laterally consistent.

Table 1: Amplitude characteristics of the key stratigraphic horizons in 6306/6-1 and surfaces used in this study.

3.2 Structural restoration

Two-way time structure maps (**Figure 3)** generated by detailed manual interpretation of 3D seismic reflection data were depth converted using a velocity model that is based on stacking velocities (Johnson & Hansen, 1987; Marsden, 1989; Ashcroft, 2011) . The accuracy of the resultant depth converted surfaces is independently verified by wells 6306/6-1 and 6306/9-1: the difference between the depth-converted seismic horizons and their actual depth in the wells is less than 20m. We apply a crude structural restoration through a simple 'rigid body' rotation of a depth converted Top Viking Group surface is applied to remove the westward, post-rift tilting associated with continued burial and post-rift thermal subsidence throughout the latter part of the Cenozoic (Brekke, 2000; Bell et al., 2014). This provides an approximation of thetopography as it existed during the Late Jurassic. Deformation effects related to compaction and flexure during burial and post-rift thermal subsidence are expected to be minimal and consistent across the study since the area of interest (15 x 20 km) is substantially smaller than the flexure of the Norwegian margin during post-rift subsidence (Brekke, 2000; Bell et al., 2014).

4 Seismic mapping

The seismic-to-well tie generated for 6306/6-1 (**Figure 2**) is used to characterise the seismic expression of three key stratigraphic contacts: Basement, base Viking Group and top Viking Group/'BCU'. All three reflectors are mapped with high confidence in the eastern part of the seismic reflection survey (**Figure 3**).

4.1 Top Basement TWT structure map

The contact between crystalline basement and sedimentary cover corresponds to a positive impedance contrast and a high amplitude, peak (red) reflection where basement is overlain directly by Upper Jurassic/Cretaceous strata (**Table 1**, **Figure 2)**. Where it is overlain by older Mesozoic strata the contact generates a reflection with lower amplitude **(Figure 2, 3)**. The seismic expression of the top Basement reflector can therefore be used to help distinguish whether basement is overlain by Upper Jurassic/Cretaceous strata or older Mesozoic strata **(Figure 2, 3)**. In the eastern part of the study area the top Basement surface underlies the Late Palaeozoic – Mesozoic infill of the Froan Basin **(Figure 1c, 4)**. There, the contact between basement and sedimentary cover is a non-conformity, relatively smooth, and dips to the east (e.g. **Figure 1c, 4**). In the western part of the study area the basement surface is part of the footwall scarp of the KFC generating the Frøya High (**Figure 3a**). Here, the basement surface dips to the west, is strongly undulating, and is onlapped by Upper Jurassic (Viking Group) and Lower Cretaceous strata **Figure 1c**). Within the central part of Frøya High the basement surface dips to the east within a half-graben, which is informally known as the 'Almond Basin', and is overlain by pre-Upper Jurassic sedimentary strata.

4.2 Base Viking Group TWT structure map

The base Viking Group surface commonly represents a positive impedance contrast and is expressed mostly as a peak (red) event, but its seismic expression is variable, and it may be expressed as a trough (blue) event locally (Figure 2). This variable expression is related to the unconformable nature of this stratigraphic contact, juxtaposing different lithologies across the contact.

The base Viking Group surface is relatively smooth and dips to the northwest across much of the Frøya High and margin of the Froan Basin where the Viking Group overlies the Middle Jurassic conformably. However, with greater proximity to the Frøya High the base Viking Group is increasingly recognised as an an angular unconformity (**Figure 1c, 2, 4**). Biostratigraphy from 6306/6-1 and 6306/9-1 records a hiatus across this surface that may span the Bajocian (Statoil, 1994. In areas along the southern part of the Frøya High, and underlying a N-S oriented concave-up trench on the western edge ofthe Froan Basin, the Base Cretaceous Unconformity ('BCU') has eroded down to the pre-Upper Jurassic interval. As a result, the Base Viking Group surface is coincident with the Top Basement surface where Middle Jurassic stratigraphy is absent ("deeply eroded" areas on **Figure 3b**).

The distribution of the Viking Group is more complex on the Frøya High than in the Froan Basin. Where the Viking Group is preserved it may rest either on crystalline basement, or on Lower Mesozoic stratigraphy (e.g. **Figure 4**). The latter form is most common, especially overlying the Almond Basin where the greatest areal extent of Viking Group stratigraphy is preserved on the Frøya High (**Figure 5**). Where the Viking Group overlies the Permian and Middle Jurassic of the Almond Basin, the Base Viking Group surface is an angular unconformity of around 15 degrees with older stratigraphy within the Almond Basin (**Figure 4**). Upper Jurassic, Viking Group stratigraphy noticeably onlaps relative palaeo-highs on the central and western part of the Frøya High as well as three small (1 – 2.5 km wide) highs on the eastern part of the Frøya High on the flank of the Froan Basin (**Figure 3b**)

4.3 Top Viking Group (BCU) TWT structure map

The top Viking Group/'BCU' surface marks a negative impedance contrast and corresponds to a trough (blue) event at the intersection with 6306/6-1. However, it's amplitude changes spatially recording the variable lithology of underlying and overlying stratigraphy **(Figure 2)**. It represents an erosional surface that is generally broadly parallel to the underlying strata across much of the Frøya High and margin of the Froan Basin, but locally is a down-cutting surface, eroding deeply into the substrate, that has a concave-up geometry with relief of 50-200 m in parts of the southern Frøya High and within the Froan Basin (X on **Figure 3c, 4**). Overall, the surface deepens to the west with localised regions of steepening gradient along the eastern edge of the Almond Basin, and along a N-S running ridge 2 – 3 km west of the western edge of the Almond Basin (D on **Figure 3c**). There are several regions of onlap onto relative palaeo-highs, typically 1-5 km in diameter and ~40-50 m high on the eastern side of the Frøya High, and a small cone shaped, 2 km wide region west of the Almond Basin across an area of steepening gradient of the BCU (**Figure 3c**).

4.4 The Viking Group isopach map

The Viking Group isopach map reveals substantial spatial variability in thickness (**Figure 3a**) with a relatively large, 20 km wide, depocentre overlying, and east of the previous Almond Basin (Depocentre O; **Figure 5a**), with *ca.* 150 m of Viking Group stratigraphy. In the southern part of the Almond Basin these strata are truncated and deeply eroded by the BCU forming a ~15 km long, 10 km wide depression that cuts down progressively deeper towards the south-west reducing the thickness of the Viking Group to <10 m and locally making it absent (**Figure 3b,3c, 4, 5a**). A few kilometers to the east of the Almond Basin are three accumulations of Viking Group strata up to 300 - 250 m thick each measuring *ca.* 5 km in width (Depocentres A, B and C; **Figure 5a**). These accumulations show approximately fan-like geometries in plan view, with radial thinning from their centrses and are separated by narrow (1-3 km) wide regions of zero or very limited thickness (Areas **I**, **II**, and **III** **Figure 5a**). Immediately east of these wedges angular truncations of Upper Jurassic (Viking Group) and Middle Jurassic stratigraphy and a substantial decrease in Viking Group thickness suggest widespread erosion along a N-S trending depression (Figure 4b, Figure 5). The N-S depression (Area E; Figure 4b) has a a jagged western edge, approximately 25 km long and 3-5 km wide with a maximum relative depth of ~500 m (Area E; **Figure 5b**). Farther to the north-east, closer to the centre of the Froan Basin, the Viking Group is preserved and exhibits a relatively uniform thickness between 30 – 40 m over a 5 x 5 km area (Depocentre D; **Figure 5a**). Overall, the variable thickness patterns are interpreted to represent both non-uniform deposition in Jurassic times and subsequent erosion during the Early Cretaceous.

4.5 The Cromer Knoll Group isopach map

The top of the Viking Group, commonly referred to as the BCU, marks the base of the Cromer Knoll Group isopach. The BCU is marked by onlap by the lowest part of the Cromer Knoll Group in parts of the crestal areas of the Frøya High (e.g., D in Figure 4c) and is conformable within areas on the eastern margin of the Frøya High and in the Froan Basin (e.g. F in Figure 4). The Cromer Knoll Group is relatively thin (25 m or less) or absent over the crestal and eastern part of the Frøya High (Area A, Figure 4). . Conversely, in the Froan Basin to the east there are substantially thicker accumulations of Cromer Knoll Group stratigraphy (Area E and F, **Figure 4, 5b**). The large, N-S trending erosional feature hosts up to 500 m of Cromer Knoll stratigraphy which onlaps the BCU within Area E, becoming generally thicker towards the south of and east of the feature (**Figure 4, 5b**). To the northeast within the Froan Basin, thicknesses of up to 300 m of Cromer Knoll group are observed (**Area F on Figure 5b)**.

This spatial pattern of thickness of the Cromer Knoll Group and onlap is interpreted to reflect the progressive flooding of the Frøya High, with the Frøya-Froan margin and the crestal part of the Frøya High being one of the last areas to be flooded during the early Cretaceous (Brekke et al., 2000; Bell et al., 2014; Jones et al., 2020). Unlike the Viking Group isopach map, the lateral variability in thickness of this interval is attributed mostly to non-uniform deposition on a variable underlying topography with the majority of the Lower Cretaceous deposits of the Cromer Knoll Group being non-erosional and internally conformable for the most part. The Froan Basin in the easternmost part of the study area continued to receive sediment since earliest Cretaceous times (Depocentre F; **Figure. 5b**; Skarbø et al., 1988). The large, N-S-trending erosional feature is interpreted to have been excavated during the early stages of the Early Cretaceous by the removal of Upper Jurassic and older strata had become filled by the end of the Early Cretaceous as evidenced by onlap of Cromer Knoll reflections onto the BCU on either side of the erosional depression (Depocentre E; **Figures. 5b, 4**).

5 Seismic and wellbore stratigraphy and geomorphological characterization of the Viking Group on and around the Frøya High

Observations

The seismic stratigraphic architecture within the Viking Group fan-shaped, wedges (A, B and C; Figure 5a) is relatively complex in comparison to the expression of the Viking Group elsewhere (Figure 6). By flattening the seismic on the Top Cretaceous horizon (Top Shetland Group) we can approximately restore the orientation of the reflectors that make up the wedge to their original geometry before the area became tilted towards the west (Figure 7). On the flattened data, the western and upper part of the wedges consists of parallel, horizontal to sub-horizontal reflections that onlap the basement/base Viking Group surface to the west. To the east, the wedges consist of east-dipping, inclined, sigmoidal reflections that downlap the basement/base Viking Group (**Figure. 4, 6, 7**). The maximum (non-decompacted) thickness of the wedges amounts to ~250meters (**Figure. 4, 7a**) and the internal sigmoidal reflectors dip *ca*. 10 degrees. Heights of inclined reflectors vary from ~30 – 200 m. When viewed in aNE-SW section u, reflections have apparent dips in opposing directions, away from the approximate centre of each wedge and generate broadly convex-up internal morphology with internal complexity and surfaces marked by downlaps (**Figure 8**).

Well 6306/9-1 penetrates Wedge B and recovers approximately 155 m of Middle to Upper Jurassic which lies directly on crystalline basement (**Figure 9**). Biostratigraphic and sedimentological analysis of sidewall cores are integrated with wireline and borehole image data into a summary log in Figure 9. The Middle Jurassic stratigraphy comprises a sub-horizontally bedded basal section following bed restoration, from ~941-967 m depth, of interbedded fine-medium-grained sandstone and siltstone rich in carbonaceous material and root traces, which is capped by a coarser grained, upward fining gravelly sandstone rich in carbonaceous material but also calcareous shell fragments (**Figure 9**). Palynological observations in this section show substantial presence of brackish water indicators typical of a marginal marine assemblage and is dated as Callovian. The basal section transitions abruptly at ~940 m depth into a clay-rich, non-bioturbated siltstone with low palynological diversity at the onset of a largely silt and clay-prone, ~45 m thick Oxfordian section becoming increasingly bioturbated and sand-prone upwards (**Figure 9**). This is overlain by an abrupt transition at 895 m into sand-prone sidewall core samples and consistently low gamma-ray values with a marked reversal in neutron-density separation (**Figure 9**). This section is dated as Kimmeridgian-Volgian with extensive reworking of Oxfordian palynomorphs and coincides with the position of well recognised eastward dipping, downlapping reflections in the seismic data (**Figure 6**). In the well, this is recognised as a change of restored bedding dips to steeper (*c*. 25°), exclusively eastward dips. The Kimmeridgian section can be split into three subunits (**Figure 9**) comprising medium-very coarse sandstone-prone packages separated by the shallower dipping (*c.* 10°) 1-2 m thick argillaceous sandstone beds. The three sub-units broadly demonstrate a steepening to shallowing restored bedding trend punctuated by shallower restored bedding within the intervening argillaceous sandstone intervals (**Figure 9**). Sandstone beds are typically coarse-grained, granule-bearing and poorly sorted, with occasional development of cross-stratification and abundant organic material. The section returns at 847 m depth to dominantly fine-to medium-grained sandstone that is still granule-bearing and displays planar to cross-stratification coincident with a move into shallowly eastward dipping, planar reflectors in seismic section (**Figures 6, 9**). However, this package ultimately becomes Ryazanian aged and increasingly rich in glauconite pellets and is more intensely bioturbated (*Chondrites* and *Palaeophycus*). This is capped at 819 m depth by a relatively thin, 7 m section of intensely bioturbated, coarse to very coarse, sub-horizontally bedded sandstone (**Figure 9**). The sandstone itself is overlain by gravel- and pebble-rich sandstones (813 – 815 m) with broken shell fragments and heavy minerals that account for extremely high gamma readings (**Figure 9**). This is overlain by a sub-horizontally bedded claystone with pervasive *Chondrites* at 812 m depth, coinciding with the position of the strong negative amplitude associated with the Top of the Viking Group in seismic (**Figures 6, 9**)

The Top Viking Group/BCU structure map and isopach maps show that the eastern edge of the wedges has an irregular, jagged, erosional, appearance in plan view marking the edge of the N-S erosional feature highlighted by the base of Depocentre E (X in **Figure 3c, 10**). The N-S erosional feature has connection along its western edge to 0.5 – 1.5 km wide, smaller scale erosional features trending NW-SE or E-W, which shallow to the west onto the Frøya High. The irregular nature of the BCU at the eastern edge of the wedges also hosts numerous, relatively small (*ca.* 100 m wide and 500 m long), amphitheatre-shaped depressions that shallow westwards (**Figure 10**). **I**sopach maps reveal that the Viking Group is thinner within these features (**Figure 5a, 10**) and that they are filled in with, younger, Cromer Knoll stratigraphy, that onlaps this surface (**Figure 5b, 10b**).

<u>Interpretations</u>

We interpret the Viking Group wedges with their internal sigmoidal reflections as clinoforms. Based on their fan-shaped plan view geometry of the three wedges (A, B,and C and D; **Figure 5a, 7**) and eastward dipping and prograding foresets, the wedges are interpreted as eastward prograding deltaic packages. Observations of carbonaceous, rooted heterolithic sandstones from 6306/9-1 suggest the deltaic clinoforms are preceded by a Callovian-aged coastal plain containing occasional fluvial channels which became transgressed in the Oxfordian establishing a largely dysoxic, mud-prone shelf and increasingly sand-prone prograding shoreface rich in bioturbation. This backstepping is followed by the strongly progradational deltaic clinoforms observed on seismic (**Figure 6, 7b**) which are seen to be that of a coarse-grained sand-prone and poorly sorted, eastward prograding delta initiated during the Kimmeridgian (**Figure 9**). The observed height and relatively steep (>10°) angle of the clinoform foresets indicates progradation into a waterbody up to ~200 m deep towards the upper, later part of the Viking Group section. Smaller foresets (from 30-50 m) during the onset of the clinoform packages (Figure 6) indicate periods of less accommodation early in the history of the deltas increasing in height through younger clinoforms, with foreset height through the deltas depending on the interaction of sea-level and seafloor topography at a given time (**Figure 7, 9**). Argillaceous sandstones intersected in the wells demonstrate similar thicknesses and characteristics to reactivation surfaces separating foreset packages documented in fan deltas (e.g., Backert et al., 2010; Gawthorpe et al., 2017; Barrett et al., 2019). Similarly, the scales (10-30 metres thick) and lithology (coarse-grained, gravel-pebble prone sandstones) of the steeper cross-stratified sub-units are comparable to thatof Gilbert-type fan deltas with steeply dipping delta fronts comprising a broad range of gravity flow deposits (Massari & Collela, 1988; Nemec, 1990; Rohais et al., 2008; Gobo et al., 2014; Barrett et al., 2019; Chiarella et al., 2020).

The arcuate, amphitheatre-shape of some of the erosional features (**Figure 5, 10**) resemble the scars left by slumping of unconsolidated material observed on modern subaqueous depositional slopes (e.g., Biscara et al., 2012; Gales et al., 2019) and in outcrop (Postma 1984; Backert et al., 2010; Gobo et al., 2014; Rubi et al., 2018). Similarly, they could also represent longer lived tributaries into the larger N-S directed erosional features. The current dataset is not sufficient to conclude whether the N-S-trending erosional feature (Area E; **Figure. 4, 5b, 5**) formed concomitant with the clinoform package or if it is a younger and distinct, separate feature. However, the main erosional surface of the BCU is locally underlain by slightly older, intra-Late Jurassic erosive features within the northern most part of Depocentre E (Figure 5b, 7d) suggesting that the head of this feature may have initiated during the Late Jurassic, with minor periods of filling, prior increased erosion as part of a larger, subaqueous drainage system during the Cretaceous.

6 Structural restoration of the Late Jurassic rift terrain

The Upper Jurassic clinoform packages on the Frøya High, particularly their topsets that were deposited in a near-horizontal coastal plain or shallow marine platform setting, may provide constraints on the amount of tilting that has occurred since Late Jurassic times.

Figure 11 shows the depth-converted section rotated by 20 degrees on the basis the western flanks of the clinoform packages are interpreted to be sub-horizontal topsets during the Late Jurassic. The resultant section (**Figure 11c**) represents an approximation of the attitude of sedimentary rocks of the Viking Group on the Frøya High at the time of deposition (Figure 12). Our simple approach does not incorporate flexure and compaction and isless accurate away from the anchor point, Viking Group wedge 'B' on **Figure 5a**, and especially where uplift would be greater, closer to the KFC. Additionally, the Top Viking Group/BCU structure map is a composite surface which in places is conformable (e.g., near 6306/6-1 and 6306/9-1), but in others reflects substantial erosion (e.g., areas marked '1', '2' and '3' on **Figure 12**.). In areas where the Viking Group was partially removed during the post-rift phase the surface contains topographic elements that post-date the Jurassic and so may not reflect the Late Jurassic configuration of the surface within those specific areas. Despite these shortcomings of our simple approach, the restoration of **Figure 11, 12** performs well in the eastern flank of the Frøya High and within the clinoform packages where there is limited post-Late Jurassic erosion. The restoration suggests that a prominent irregularity on the basement contact immediately west of the Almond Basin ('y' in **Figure. 11b**) formed a topographic high during late Jurassic times (**Figure 11c**). The thickness maps of **Figure 5** reveal that this topographic high corresponds to an area of non-deposition during the Late Jurassic (**Figure 5a**) and to some extent also during the Early Cretaceous (**Figure 5b**). Together, these observations suggest that this north-south trending basement ridge likely represented the apex of the Frøya High during the Late Jurassic seen in both the Viking Group thickness map and the restored Top Viking Group structure map (**Figsures 5a and 12**). We interpret this ridge to represent the drainage divide of the Frøya High as it existed during Late Jurassic- and possibly Early Cretaceous times (**Figure 3**).

7 Late Jurassic palaeo-drainage and palaeogeography of the Frøya High

The interpreted prograding shoreline-delta system developed east of, and parallel to, the eastern margin of the Almond Basin. The structural restoration of **Figure 12** suggests that the Almond basin was positioned topographically higher than the clinoform packages during Late Jurassic times and was likely subaerially exposed when the clinoform packages were prograding. In addition, the interpreted palaeo-drainage divide of the Late Jurassic was located parallel to and immediately west of the Almond Basin. These interpretations together allow constraint on the position and geometry of the palaeo-catchments which fed the clinoform packages, and broadly encompass the area 'O' in the Upper Jurassic thickness map of **Figure 5a**.

Each of the distinct Upper Jurassic clinoform packages (A, B, C in **Figure 5a, 13**), are connected to to the central portion of the Frøya High (Area O – Figure 5a) through three, substantially thinner, but narrow corridors of Upper Jurassic deposits (**Figure 5a**). Each of these narrow corridors are separated by areas where the Upper Jurassic stratigraphy is extremely thin (<20 m) or largely absent (**I**, **II** and **III** on **Figure 5a**). In these areas (**I**, **II** and **II** on Figure 5a) the strong negative acoustic impedance, linked to organic rich shales typical of the Top Viking Group is still preserved (e.g., intersection with Area **II** in **Figure 7b**), and so indicates these areas do not simply represent enhanced Early Cretaceous erosion unlike deeply eroded areas of Viking Group stratigraphy. We interpret the thickness patterns of the Viking Group to reflect thatthe geometry ofpalaeo-catchment area 'O' (**Figure 5a**) was likely subdivided into a series of parallel drainage catchments with SE-flowing river systems that debouched to the southeast and supplied sediment to individual point-sourced fan deltas between areas **I**, **II** and **III** (**Figures 5a and 13**). The area occupied by the palaeo-catchment on the restored structure map of **Figure 12** is affected by Early Cretaceous erosion, which renders it inadequate for mapping more subtle features of Late Jurassic such as individual drainage profiles. However, the restoration does provide some constraints on overall catchment geometries.

Measuring from the maximum eastern (basinward) extent of the Viking Group thickness anomalies to the interpreted drainage divide provides an approximate maximum catchment length of 12.5 km, 16.9 km and 18.3 km for clinoform package A, B and C respectively with a mean catchment length of 15.9 km (Supplementary Information). The catchment for clinoform package D is only partly covered by the dataset and so the length is difficult to constrain. The total basinward extent of the Viking Group thickness anomaly probably overestimates the catchment length as it inclues a portion of subaerial topset, subaqueous foreset and bottomset which is not part of the subaerial catchment (Hovius, 1996). Alternatively, the location of catchment outlets can be estimated from the isopach map as the region where there is an abrupt widening and onset of a fan-like geometry of the thickness anomalies. Using the estimation of the catchment outlet provides a minimum estimate of the catchment length which are

8.0, 11.3, and 12.1 km for clinoform package A, B and C respectively, giving an average length of 10.5 km, and indicating an average clinoform package length of 5.2 km (Supplementary Information). These dimensions are in keeping with ancient and modern deltaic clinoforms observed in the Corinth Rift (e.g., Barrett et al., 2019), and measurements in compiled database studies for sand-prone deltaic clinoforms (Patruno et al., 2015).

The spacing between catchments can be roughly estimated using the small, 1-5 km long, ~100 m high,relative highs (I, II and III on **Figure 5a** and **Figure 13a)**and assuming that the catchment outlets were located centrally between them. This analysis gives catchment spacings of 5.7 km between C and B, and 7.6 km between B and A, averaging 6.7 km, or 6.3 km if the Viking Group thickness anomaly (Wedge D) north of Wedge A, to the west of 6306/6-1 is also included (Supplementary Information). The spacing ratio of catchment length to spacing averages 1.69 using minimum length estimates, and 2.4 using maximum length estimates, in keeping with catchment area morphometrics for active basins in other studies (2.07 – Hovius, 1996; 2.5 – Talling et al., 1997; 2.48 Sømme et al., 2010). The area of the catchments ranges between 44 – 104 km^2, which is typical for small catchments common in active rift margins (e.g., Eliet & Gawthorpe, 1995).

Characterisation of the Frøya High bedrock stratigraphy highlights that Late Jurassic catchments consisted of relatively easily erodible sedimentary rocks of Upper Palaeozoic – Lower Mesozoic age within the Almond Basin, as opposed to the crystalline rocks elsewhere, outside the Almond Basin, on the southern Frøya High (Jones et al., 2020; Munoz-Barrera et al., 2020, 2021). We conclude on the basis of spatial patterns of Viking Group thickness, the position of a NE-SW trending ridge following restoration, and comparison with other rift system catchment morphometrics, that the interpreted Upper Jurassic clastic shoreline system was supplied by at least four distinct drainage basins, each around ~10 km, long spaced 5.5 – 7.5 km along the dip slope of the Frøya High. Each drainage basin was preferentially located on exposed pre-Middle Jurassic sedimentary rocks of the Almond Basin which provided easily erodible material feed clinoform packages that prograded eastward into the Froan Basin.

8 Early Cretaceous evolution of the Frøya High

The erosional features of the Top Viking Group/BCU surface removed substantial portions of the Upper Jurassic stratigraphy (e.g. Area 1 – 5 on **Figure 12, Figure 13b**). The timing of this erosion is poorly constrained and it is possible that it could have commenced during the end of the latest Jurassic (e.g. sub-BCU erosive features on **Figure 7d**) .. Areas 1 – 3 exhibit a broadly N-S-orientation, compared to E-W orientation of the Late Jurassic drainage catchments (**Figure 12 Figure 13**). Moreover, these areas seem to represent catchments that drain towards the southwestern edge of the Frøya High. Areas 4 and 5, however, have the same location and orientation as their corresponding Late Jurassic erosional features (Figure 12, 13). It thus follows that those catchments that drained westward into the Møre Basin were not rearranged during the transition from the Late Jurassic to the Early Cretaceous. Those Jurassic catchments (Areas 1 – 3) that used to be contained within the east-facing dip slopedip slope, however, underwent significant change. A clear indication of the mechanism behind this rearrangement of drainage on the dip slopedip slope is suggested by Area 3 (**Figure 13b**), where headward erosion from one of the fault scarp-bounded catchments (**3 on Figure 12 and 13b**) appears to have captured a large portion of the catchment that was previously draining eastward. The final form of the erosive features (e.g., 1-5 on **Figure 13b**) is interpreted to be of Early Cretaceous age as large portions of Upper Jurassic stratigraphy that covered the Almond Basin, likely deposited during transgression of the Jurassic drainage basin ('O' in **Figure 5**), were eroded by the younger, southward draining catchment. We propose that this must have occurred as the footwall scarp catchments along the KFC continued to grow by headward erosion.

Although the relatively deep, southward directed canyon immediately east of the clinoform package (Area 2, in **Figure 12**) extends south beyond the study area it seems plausible to be the result of a similar drainage capture event that could have occurred farther to the southeast along the KFC fault scarp. Observations of degradation of the delta foresets, and of sub-BCU erosion in the northern part of this erosive feature (e.g., Figure 7d) indicate that the Area 2 canyon may have begun forming whilst the clinoform packages were active during the Latest Jurassic. Here, degradation of the clinoform delta-front may have facilitated sediment transport into and along the basin floor in an axial channel system not dissimilar to axial channels observed in front of modern fan deltas (e.g. Prior & Bornhold, 1989; McNeill et al., 2005; Beckers et al., 2018; Gales et al., 2019; Gawthorpe et al., 2018). However, the data is not able to resolve how much of this erosion substantially post-dates the emplacement of the clinoform packages (i.e during the Early Cretaceous), and is formed by more widespread, headward, subaqueous erosion of the then submerged Frøya High flank. Nevertheless, the isolated positions of Cromer Knoll Group thicknesses and onlap of the Cromer Knoll Group onto the BCU suggest that the topography of Area 2 within the canyon was in place by the end of the Early Cretaceous (**Figure 4, 7, 13)**.

The canyon at Area 2 likely formed a substantial topographic/bathymetric low within which the Cromer Knoll Group was deposited (**Figure 13**) and may well have formed through a composite history of both Late Jurassic and Early Cretaceous erosion. The Lower Cretaceous Cromer Knoll Group in the study area consist of continuous, sub-parallel strata that onlaps the BCU with some minor concave-up geometries within the broad N-S orientated erosional feature (Area E, **Figure 4, 6, 7d**). The lack of any major constructional features along the flank of the Frøya High (cf. Upper Jurassic clinoform packages) suggests that the Frøya High depositional systems which routed sediment towards the Froan Basin likely shutdown and that sediment routing was largely focussed to the south and west of the Frøya High through the Early Cretaceous. A termination of sediment supply from region O (**Figure 5)** is in agreement with the gradual onlap of the Frøya High by the Cromer Knoll Group, recording a relatively fast transgression of the Frøya high at the end of the Jurassic and into the Early Cretaceous (**Figure 3c**; **9**; Brekke, 2000; Bell et al., 2014; Jones et al., 2020).

9 Discussion

9.1 Alternative interpretations of the studied clinoform packages: The Rogn Formation as a connected, constructional coastline on the Frøya High

Our interpretation of the Upper Jurassic packages on the southeastern part of the Frøya High as deltaic clinoform packages is different from earlier interpretations. Chiarella et al. (2020) propose the same sand-prone packages within the Rogn Formation to be interpreted as coastal sand ridges sourced and constructed solely through longshore currents, using comparisons between core from the well 6306/6-1 and the Draugen field 100-125 km to the north-east (also described by Van der Zwaan, 1990). Deltaic clinoforms are our preferred interpretation on account of the lobate, convex to the east plan view geometry, eastward progradation, consistent with an overall upward coarsening, poorly sorted, coarse-grained foreset-dominated package in 6306/9-1 (**Figure 9)**, typical of fan deltas (e.g., Nemec 1990; Rohais et al., 2008). Furthermore, the location of the clinoform packages down-dip of a prominent, erosional, drainage catchment-liked geometries, floored by highly erodible sedimentary deposits of the Almond Basin implies the bulk of sediment was deposited within deltas at the coastline with only minor reworking and northward transport of sediment within delta topset deposits (e.g., Figure 9, Figure 13, 14). The clinoform packages all exhibit a consistent progradational architecture from west to east, with parallel topsets overlying or connected to generally east-dipping sigmoidal clinoforms when Upper Mesozoic and Cenozoic rotation is removed by flattening onto a Top Shetland Group horizon (**Figure 7**). Chiarella et al. (2020) do refer to westward dipping foresets in the northernmost post of the dataset, immediately west of 6306/6-1. However, we observe only a single westward dipping surface (**Figure 7d**) which ties downdip into the large N-S trending erosional feature (e.g. Depocentre E, **Figure 5**). We therefore interpret this westward dipping reflector to be the margin of the up-dip head of this erosional feature that post-dates the delta itself. The consistent eastward progradation is more compatible with that of a radial fan delta than with an offshore sand-ridge, which would likely show coastline parallel progradation. Whilst progradational clinoforms do form within offshore sand ridges (e.g., Berne et al., 1998) their angle is typically less than 10 degrees, and foreset heights rarely exceed 30 meters (Chiarella et al., 2020), an order of magnitude smaller than the maximum height of those observed in the Frøya High study area. The abundance of bioturbated, macro-fossiliferous, plant material-rich facies of the Rogn Formation described in 6306/6-1 by Chiarella et al. (2020) and used to ascribe a sand-ridge interpretation are not necessarily unique to that depositional environment. Bioturbation, macro-fossil and plant-material rich sandstones are common in a broad range of shoreline and near-shoreline depositional environments and are especially common in wave- or tide-modified delta fronts (Gustaldo & Huc, 1992; Rossi & Steel, 2015; Annell et al., 2020)..

Our interpretation of the studied Upper Jurassic clinoform packages as a series of fan deltas has implications for the overall depositional setting and sediment flux across the eastern flank of the Frøya High during the Late Jurassic. **Figures 13 and 14** illustrate a new, depositional model that shows a coastline along the eastern side of the Frøya High that is more constructive and dominated by transverse sediment input, rather than axial reworking that has dominated previous models driven by observations from the Draugen sand ridge (e.g. Van der Zwaan, 1989; Chiarella et al., 2020). Palaeocurrent measurements from 6306/9-1 do suggest a component of longshore reworking near the top of the Rogn Formation, however we interpret this to be limited to reworking within the topsets of deltas, with the large thicknesses of sediment within the proposed deltas suggesting considerable volumes of sediment are stored within the deltas rather than transported further northwards.

Whilst the existence of shallow marine systems flanking the transition between the Frøya High and Froan Basin have long been speculated on the basis of observations from the Draugen Field (Van der Zwaan, 1989: Chiarella et al., 2020), we speculate further that the Draugen sand ridge may be more intimately related to the regressive, deltaic shoreline documented here. Existing interpretations for sedimentation of the Draugen Ridge lacked a demonstrable sedimentary input for sediment reworked axially from the southwest. The proto-Norwegian Sea existed as a narrow seaway located above 30 degrees latitude from the early through to the Late Jurassic. Palaeoclimate interpretations for the Late Jurassic and Early Cretaceous of the North Sea and NW Europe (e.g. Abbink et al., 2001; Mutterlose et al., 2003) highlight that the prevailing current direction was controlled by the northern hemisphere westerlies, i.e. directed to the north east. These current directions are consistent with the dune migration direction proposed in Chiarella et al. (2020) for the asymmetry of the Kimmeridgian Rogn Formation at the Draugen field, and with Early Jurassic Ilje Formation shallow-marine bar progradation, and long-shore sediment redistribution in the Halten Terrace (Martinius et al., 2001). As a result of these westerlies, the northwestern margin of the Frøya High likely received a strong northeastern current as the southern part of the Sklinna Ridge was submerged and formed an opening to the proto-Norwegian Sea to the west (Bell et al., 2014; Elliott et al., 2015, 2017). Similar currents along the eastern flank of the Frøya High were also likely in operation due to the same prevailing current direction, which may have been enhanced through interaction of the several exposed islands in the narrow seaway of the proto-Norwegian sea **(Figure 14)**. Petrographic information of the Kimmeridgian Rogn Formation at the Draugen ridge (Van der Zwaan, 1990; Chiarella et al., 2020) and broader Møre-Trøndelag area (Mørk & Johnsen, 2005) indicate a provenance with minor reworking from local granitic and Mesozoic-sediment covered palaeohighs such as the Frøya High to the south and west of the Draugen Ridge and Froan Basin (Jongpier et al., 1996; Mørk & Johnsen, 2005). This petrographic signature is consistent with a redistribution of sediment along strike in the shoreline region of the Frøya High – Froan basin margin, with the confluence of these currents meeting at the Draugen Ridge, on the eastern tip of the Vingleia Fault (**Figure 14**). The deltaic clinoform systems recognised in this study in the southern part of the Frøya High likely provide the primary sedimentary input for the more minor amount of sediment which may bereworked along the Frøya High-Froan basin margin. The description of the Draugen ridge presented by Van der Zwaan (1989) and Chiarella et al. (2020) along with our model of redistribution is consistent with the prediction by Nielsen & Johannessen (2009) of how spit systems will often locate at the confluence of meteorological oceanic currents around a landmass, along-strike from major sediment input points, where a majority of sediment remains. The stratigraphic architecture recognised in Chiarella et al. (2020), with a large subaqueous, mud-dominated platform on which upward-coarsening units from a subaerial, high-energy environments are deposited also bear similarities with modern and recent spit environments documented in Nielsen & Johannesen (2009).

9.2 Implications for models of clastic shoreline sedimentation on rift-related dip slopedip slopes

9.2.1 Impact of hinterland characteristics and source-to-sink configuration on depositional systems around intra-basinal highs

In the case of the Frøya High, the nature of the bounding structures and resultant physiography of the Late Jurassic landscape can produce substantial along strike variability in the nature of the coastline. This case study demonstrates that if a relatively sizeable source for sediment is exhumed during the evolution of a rift, even in an intra-basinal location, constructive coastal environments may develop locally on dip slopedip slopes, especially downslope of easily erodible sedimentary bedrock. At the southern edge of the Frøya High, a relatively broad, backtilted, footwall dip slope consisted of an easily erodible exhumed sedimentary basin (the Almond Basin) that supplied sediment to a series of closely spaced fan deltas and resulted in a regressive coastline. Less than 100 km to the north, where the Frøya high is significantly narrower and consists of resistant, crystalline bedrock, sediment supply is likely dependent on longshore drift (Van der Zwaan, 1989; Chiarella et al., 2020). The longshore drift dominated coastlines in this region may be dominantly transgressive compared to more progradational or aggradational time-equivalent systems along-strike to the southwest. Muravchik et al. (2018) highlight the co-existence of sediment starved dip slopeand delta-fed dip slopes over strike distances of 10-20 km-from the El-Qaa fault block of the Suez Rift. Muravchik et al. (2019) suggest that the steepest structural gradients and greatest uplift, towards the centre of fault segments drive the location of primary sediment input points on dip slopes, whereas shallower structural gradients around fault tips are more likely to be easily transgressed by rising sea level and sediment starved. Our findings indicate that, in addition to structural changes, the width and bedrock composition of the dip slope are important factors to consider in controlling sediment supply, the nature of the dip slope coastal plain, and shallow marine regime. Narrow exposed zones of dip slopes, without the development of drainage catchments, may not be able to contribute significant sediment yield in order to build constructive coastlines (**Figure 15a)**. Broader dip slopes can develop larger catchments and potentially connect to greater altitudinal differences from headwaters to drainage outlet, with consequently greater discharge and erosional capability from steeper drainage profiles (Sømme et al., 2009; Romans et al., 2016; Nyberg et al., 2018). dip slope Nevertheless, the sediment yield is likely to be relatively small given the shallow angle of dip slopes (0-7°, Muravchik et al., 2018) compared to steeper catchment systems developed on the footwall scarp of normal. Slower subsidence rates, shallower gradients and shallow water depths make dip slope systems prone to be constructional depositional systems unlike steep, deep fault-attached systems in the immediate hangingwall of major normal faults (Gawthorpe et al., 1994; Ravnås & Steel, 1998; Rapozo et al., 2021; Smyrak-Sikora et al., 2021). For example, the Viking Group in the hangingwall of the major faults (KFC and VFC) that bound the Frøya High are dominated by deep-water fans and bypassed fault scarps with limited capacity for shelfal development or shoreline sediment storage (Elliot et al., 2015, 2017; Jones et al., 2020). The tectonostratigraphic setting of constructive shorelines on the low gradient, back-tilted footwall dip slopes may record substantially different stratigraphic architecture and depositional stacking patterns due to their increased sensitivity to eustatic base-level changes compared to depositional systems in the immediate hangingwall of a major normal fault (Leeder & Jackson, 1993; Gawthorpe et al., 1994, 2017; Ravnås & Steel., 1998; Jackson et al., 2005; Henstra et al., 2017; Barrett et al., 2018; Smyrak-Sikora et al., 2021). dip slope

9.2.2 Impact of the structural configuration of dip slope systems

Other dip slope systems (e.g. El-Qaa and Hammam Faraun Fault Blocks, Gulf of Suez (Jackson et al., 2005; Muravchik et al., 2018); Snorre-H area and, Central Graben of the North Sea (Nøttvedt et al., 2000); Upper Heather Member, Oseberg Fault Block (Ravnås et al., 1997; Ravnås & Steel., 1998)), all exhibit a net-transgressive character from drowning of the dip slope similar to the capping of the deltas here by a transgressive section (**Figure 9**). Large scale, terminal flooding occurs because of continued rotation and net subsidence of the dip slope in response to either to background-subsidence of the margin and cessation of fault, or enhanced activity in the hangingwall of a nearby fault (e.g., Ravnås et al., 1997; Ravnås & Steel., 1998). Unlike other published examples, all the clinoforms observed on the Frøya High show strongly progradational character, and we observe no backstepping of deltaic units at the seismic scale prior to their termination. Observations in 6306/9-1 demonstrate a well-developed delta topset which is abruptly flooded with a thin transgressive-lag overlain by offshore mudstones of the Spekk Formation, rather than more gradual backstepping (**Figure 9**). This lack of protracted, terminal retrogradation suggests flooding occured abruptly due to rapid sea-level rise or drastic sediment supply reduction, which would be counter intuitive against the ongoing uplift-induced steepening of the catchment headwaters. The Abrupt transgression of the Frøya dip slope systems may be at least partly explained through the drainage capture from headward erosion by catchments on the Klakk Fault Complex footwall crest (**Figure 15a)**. The Early Cretaceous timing of drainage capture to south/southwest draining catchments is simultaneous with previously documented acceleration and localisation of deformation on the Klakk Fault Complex due to its linkage to a major detachment in the lower crust (Peron-Pinvidic et al., 2013; Bell et al., 2014; Muñoz-Barrera et al., 2020). The process of drainage capture by footwall scarp drainage and reduction in dip slope catchment area may be a common rearrangement where displacement on the controlling normal fault continues or accelerates rather than transferring to other structures (Leeder et al., 2005; Privat et al., 2021).

To maintain progradational architectures without retrogradation during net subsidence however requires substantial sediment flux. The balance of sediment supply to accommodation for dip slope depositional systems will be influenced by rotation of the fault block, uplift of the catchment to steepen drainage profiles, the gradient of the subsiding (depositional) part of the dip slope, and any changes in sea-level (Gawthorpe et al., 1994; Ravnås et al., 1997; Ravnås & Steel., 1998). Dip slopes in rift basins can occur through two relationships to an active normal fault; rotation in the footwall of a major active fault (**Figure 15a**), or rotation in the hangingwall of a major active fault (**Figure 15b)**. In a footwall uplift driven system such as the Frøya High, we observe strongly progradational architectures on the dip slope prior to an abrupt termination of the system from drainage capture and flooding rather than the preservation of a gradual retrogradation and transgression of the clinoform packages. The existence of deltaic systems on the Frøya High in a depocenter approximately 20 km from the drainage divide, and 30 km from the Klakk Fault Complex, is consistent with a change to net-subsidence, due to contributions from background subsidence, at half the wavelength of flexure of most large normal faults (40-60 km; Morley, 1995; Armijo et al., 1996; Fernàndez-Blanco et al., 2020). Given the decay of uplift to subsidence away from a bounding fault across a dip slope, the uplift of a diplsope catchment closer to the fault is likely to be greater than the subsidence experienced in the dip slope further from the fault. The resultant uplift-induced steepening of the drainage profile in the upper reaches of catchments, is therefore likely to allow an increase in sediment flux which can exceed the accommodation generated by subsidence to produce the strongly aggradational to progradational character observed on the Frøya High dip slope (**Figure 15a**). Conversely, in a hangingwall subsidence driven setting (e.g., Alkyonides Gulf – Leeder et al., 2005; El-Qaa Fault Block – Muravchik et al., 2018) (**Figure 15b)**, subsidence is likely to be greater in the depocentre than uplift in the catchment feeding the dip slope depositional systems and uplift and steepening of the catchments may be very minor, or the catchment may even undergo net subsidence (Pechlivanidou et al., 2019). As a result, even coastal systems with a fluvial input become accommodation-dominated and are easily transgressed by subsidence-induced sea-level increases producing the retrograding stacking patterns observed in hangingwall subsidence driven dip slope systems such as those seen in the dip slope systems of the Alkyonides Gulf (Leeder et al., 2005), Oseberg Fault Block (Ravnås et al., 1997; Ravnås & Steel., 1998) and El-Qaa and Hammam Faraun Fault Blocks (Jackson et al., 2005; Muravchik et al., 2018). Temporal changes in fault activity (similar to the high and low 'tilt rates' of Ravnås & Steel., 1998) , and interactions with non-tectonic changes in sea-level or sediment flux have the capacity to alter this motif however the differences between hangingwall and footwall driven dipslopse systems highlights that the location of synchronous fault activity is a key controlling parameter on evolution and resultant stacking patterns.

10 Conclusions

Detailed seismic mapping and analysis of borehole data within the Viking Group in the footwall dip slopeof the Klakk Fault Complex has revealed a constructive, delta-dominated shoreline system on the eastern flank of the Frøya High. These sedimentary systems are sourced from eroded material from the eastern side of a drainage divide in the footwall of the Klakk Fault Complex that was transported eastwards down the back-tilted, footwall dip slope into the Froan Basin. This case study provides an example of the facies and stratigraphic architecture of dip slope depositional systems within rift settings and highlights spatial variations in dip slope sedimentation over 100 km along-strike.

The example on the Frøya High demonstrates the potential for intra-basinal highs to provide substantial sediment sources not only into the hangingwall of major faults, but also across the back-tilted dip slope in their footwall. Comparison with previous interpretations, and other examples of syn-rift dip slope systems, highlight the likely transient nature of coarse-grained systems on dip slopes as they respond to steepening of the headwaters of feeding catchments, which can drive high sediment flux and progradation despite ongoing subsidence further down the dip slope. We hypothesise that footwall uplift driven systems are likely to be more prone to progradation followed by abrupt shutdown resulting from drainage capture by footwall scarp drainage networks. In contrast, hangingwall driven systems are more prone to gradual transgression and form overall retrograding systems.

Integration with regional palaeogeography highlights that the deltaic packages may be important for determining the location, sediment budget and calibre of sediment supplied to longshore shallow marine systems such as spits and sand-ridges such as the Draugen Ridge. The study ultimately highlights major progradation of dip slope systems on the back-tilted footwall dip slopes of intra-basinal highs bound by high displacement normal faults, especially where bedrock is composed of easily erodible material. This is in contrast to shallower gradient low-displacement dip slope systems, or those generated in the hangingwall of large structures, which generally have more limited progradation, and preserve strong retrogradational stacking patterns.

11 Acknowledgements

This research was conducted as part of the Petromaks II Syn-Rift Systems project (255229) funded by the Norwegian Research Council and project partners (Equinor, ConocoPhillips, DNO, Neptune Energy, AkerBP and Tullow Oil). AkerBP and former Lundin Energy are thanked for permission to publish data from the 6306/9-1 well. We thank the reviewers Jonathan Obrist, Aleksandra Smyrak-Sikora and Lise Nakken for their thorough, insightful, and constructive reviews and Cari Johnson for their editorial handling of the manuscript. The authors thank Sander H Berg for discussion during the work in this manuscript. Publically released data is accessed through the UiB-DISKOS agreement. RLG thanks the VISTA programme of Norwegian Academy of Science and Letters for the award of its VISTA Professorship. GAH is now an employee of AkerBP. There are no other conflicts of interest to declare.

12 References

Abbink, O., Targarona, J., Brinkhuis, H. and Visscher, H. 2001. Late Jurassic to earliest Cretaceous palaeoclimatic evolution of the southern North Sea. *Global and Planetary Change*. 30(3), pp.231–256.

Anell, I., Zuchuat, V., Röhnert, A.D., Smyrak-Sikora, A., Buckley, S., Lord, G., Maher, H., Midtkandal, I., Ogata, K., Olaussen, S., Osmundsen, P.T. and Braathen, A. 2021. Tidal amplification and along-strike process variability in a mixed-energy paralic system prograding onto a low accommodation shelf, Edgeøya, Svalbard. *Basin Research*. 33(1), pp.478–512.

Armijo, R., Meyer, B., King, G.C.P., Rigo, A. and Papanastassiou, D. 1996. Quaternary evolution of the Corinth Rift and its implications for the Late Cenozoic evolution of the Aegean. *Geophysical Journal International*. **126**(1), pp.11–53.

Ashcroft, W. 2011. Chapter Six: Velocity analysis, CMP stacking and post-stack migration *in: A Petroleum Geologist's Guide to Seismic Reflection.* Blackwell Publishing. pp 41 – 49.

Backert, N., Ford, M. and Malartre, F. 2010. Architecture and sedimentology of the Kerinitis Gilbert-type fan delta, Corinth Rift, Greece. *Sedimentology*. 57(2), pp.543–586.

Barrett, B.J., Hodgson, D.M., Collier, R.E.L. and Dorrell, R.M. 2018. Novel 3D sequence stratigraphic numerical model for syn-rift basins: Analysing architectural responses to eustasy, sedimentation and tectonics. *Marine and Petroleum Geology*. 92, pp.270–284.

Barrett, B.J., Collier, R.E.L., Hodgson, D.M., Gawthorpe, R.L., Dorrell, R.M. and Cullen, T.M. 2019. Quantifying faulting and base level controls on syn-rift sedimentation using stratigraphic architectures of coeval, adjacent Early-Middle Pleistocene fan deltas in Lake Corinth, Greece. *Basin Research*. 31(6), pp.1040–1065.

Barrett, B.J., Hodgson, D.M., Jackson, C.A.-L., Lloyd, C., Casagrande, J. and Collier, R.E.L. 2021. Quantitative analysis of a footwall-scarp degradation complex and syn-rift stratigraphic architecture, Exmouth Plateau, NW Shelf, offshore Australia. *Basin Research*. 33(2), pp.1135–1169.

Bilal, A., McClay, K. and Scarselli, N. 2020. Fault-scarp degradation in the central Exmouth Plateau, North West Shelf, Australia.*In:* McClay, K.R & Hammerstein, J.A (eds) *Passive Margins: Tectonics, Sedimentation and Magmatism. Geological Society, London, Special Publications no.* **476**(1), pp.231–257.Biscara, L., Hanquiez, V., Leynaud, D., Marieu, V., Mulder, T., Gallissaires, J.-M., Crespin, J.-P., Braccini, E. and Garlan, T. 2012. Submarine slide initiation and evolution offshore Pointe Odden, Gabon — Analysis from annual bathymetric data (2004–2009). *Marine Geology*. **299–302**, pp.43–50.

Beckers, A., Hubert-Ferrari, A., Beck, C., Papatheodorou, G., de Batist, M., Sakellariou, D., Tripsanas, E. and Demoulin, A. 2018. Characteristics and frequency of large submarine landslides at the western tip of the Gulf of Corinth. *Natural Hazards and Earth System Sciences*. 18(5), pp.1411–1425.

Bell, R.E., Jackson, C. a.-L., Elliott, G.M., Gawthorpe, R.L., Sharp, I.R. and Michelsen, L. 2014. Insights into the development of major rift-related unconformities from geologically constrained subsidence modelling: Halten Terrace, offshore mid Norway. *Basin Research*. 26(1), pp.203–224.

Bell, R.E., Duclaux, G., Nixon, C.W., Gawthorpe, R.L. and McNeill, L.C. 2017. High-angle, not low-angle, normal faults dominate early rift extension in the Corinth Rift, central Greece. *Geology.* 46(2), pp.115–118.

Berne, S., Lericolais, G., Marsset, T., Bourillet, J.F. and De Batist, M. 1998. Erosional offshore sand ridges and lowstand shorefaces; examples from tide- and wave-dominated environments of France. *Journal of Sedimentary Research*. 68(4), pp.540–555.

Blystad, P., Brekke, H., Færseth, R.B., Larsen, B.T., Skogseid, J. and Tørudbakken, B. 1995. Structural elements of the Norwegian continental shelf. Part II: The Norwegian Sea Region. The Norwegian Petroleum Directorate.

Brekke, H. and Riis, F. 1987. Tectonics and basin evolution of the Norwegian shelf between 62°N and 72°N. *Norsk Geologisk Tidsskrift*. 67, pp.295–322.

Brekke, H. 2000. The tectonic evolution of the Norwegian Sea Continental Margin with emphasis on the Vøring and Møre Basins *In:* A. Nøttvedt, B. T. Larsen, S. Olaussen, B. Tørudbakken, J. Skogseid, R. H. Gabrielsen, H. Brekke and Ø. Birkeland, eds. *Dynamics of the Norwegian Margin Geological Society Special Publication No. 167*: Geological Society of London, pp.327–378.

Brekke, H., Dahlgren, S., Nyland, B. and Magnus, C. 1999. The prospectivity of the Vøring and Møre basins on the Norwegian Sea continental margin. *Geological Society, London, Petroleum Geology Conference series.* 5(1), pp.261–274.

Bunkholt, H.S.S., Oftedal, B.T., Hansen, J.A., Løseth, H. and Kløvjan, O.S. 2022. Trøndelag Platform and Halten–Dønna Terraces Composite Tectono-Sedimentary Element, Norwegian Rifted Margin, Norwegian Sea. *In:* Drachev, S.S., Brekke, H., Henriksen, E., Moore, T (eds.) *Sedimentary Succession of the Arctic Region and their Hydrocarbon Prospectivity, Geological Society, London, Memoirs*. **57**(1), pp.M57-2017–13.Chiarella, D., Longhitano, S.G., Mosdell, W. and Telesca, D. 2020. Sedimentology and facies analysis of ancient sand ridges: Jurassic Rogn Formation, Trøndelag Platform, offshore Norway. *Marine and Petroleum Geology.* 112, p.104082.

Corfield, S., Sharp, I., Häger, K.-O., Dreyer, T. and Underhill, J. 2001. An integrated study of the Garn and Melke formations (Middle to Upper jurassic) of the Smorbukk area, Halten terrace, mid-Norway *In:* O. J. Martinsen and T. Dreyer, eds. *Norwegian Petroleum Society Special Publications. Sedimentary Environments Offshore Norway — Palaeozoic to Recent* pp.199–210.

Coward, M.P., Dewey, J.F., Hempton, M., and J Holroyd 2003. Tectonic evolution *In:* D. Evans, C. Graham, A. Armour and P. Bathurst, eds. *The Millennium Atlas: Petroleum Geology of the Central and Northern North Sea.* The Geological Society of London, pp.17–33.

Elliott, G.M., Jackson, C.A.-L., Gawthorpe, R.L., Wilson, P., Sharp, I.R. and Michelsen, L. 2017. Late syn-rift evolution of the Vingleia Fault Complex, Halten Terrace, offshore Mid-Norway; a test of rift basin tectono-stratigraphic models. *Basin Research.* 29(S1), pp.465–487.

Elliott, G.M., Jackson, C.A.-L., Gawthorpe, R.L., Wilson, P., Sharp, I.R. and Michelsen, L. 2021. Tectono-stratigraphic development of a salt-influenced rift margin: Halten Terrace, offshore Mid-Norway. *Basin Research*. **33**(6), pp.3295–3320.Eliet, P.P., Gawthorpe, R.L. 1995. Drainage development and sediment supply within rifts, examples from the Sperchios basin, central Greece. *Journal of the Geological Society, London.* 152. pp. 883-893.

Færseth, R.B. 1996. Interaction of Permo-Triassic and Jurassic extensional fault-blocks during the development of the northern North Sea. *Journal of the Geological Society.* 153(6), pp.931–944.

Færseth, R.B. 2021. Structural geology and basin development of the Norwegian Sea. *Norwegian Journal of Geology*. 100, 202018

Fernández-Blanco, D., Gelder, G. de, Lacassin, R. and Armijo, R. 2020. Geometry of Flexural Uplift by Continental Rifting in Corinth, Greece. *Tectonics.* 39(1), e2019TC005685.

Gales, J.A., Talling, P.J., Cartigny, M.J.B., Clarke, J.H., Lintern, G., Stacey, C. and Clare, M.A. 2019. What controls submarine channel development and the morphology of deltas entering deep-water fjords? *Earth Surface Processes and Landforms.* 44(2), pp.535–551.

Gawthorpe, R.L. and Leeder, M.R. 2000. Tectono-sedimentary evolution of active extensional basins. *Basin Research.* 12(3–4), pp.195–218.

Gawthorpe, R.L., Fraser, A.J. and Collier, R.E.Ll. 1994. Sequence stratigraphy in active extensional basins: implications for the interpretation of ancient basin-fills. *Marine and Petroleum Geology.* 11(6), pp.642–658.

Gawthorpe, R.L., Andrews, J.E., Collier, R.E.L., Ford, M., Henstra, G.A., Kranis, H., Leeder, M.R., Muravchik, M. and Skourtsos, E. 2017. Building up or out? Disparate sequence architectures along an active rift margin—Corinth rift, Greece. *Geology*. **45**(12), pp.1111–1114.

Gawthorpe, R.L., Leeder, M.R., Kranis, H., Skourtsos, E., Andrews, J.E., Henstra, G.A., Mack, G.H., Muravchik, M., Turner, J.A. and Stamatakis, M. 2018. Tectono-sedimentary evolution of the Plio-Pleistocene Corinth rift, Greece. *Basin Research*. **30**(3), pp.448–479.

Gernigon, L., Franke, D., Geoffroy, L., Schiffer, C., Foulger, G.R. and Stoker, M. 2020. Crustal fragmentation, magmatism, and the diachronous opening of the Norwegian-Greenland Sea. Earth-Science Reviews. 206, p.102839.

Gobo, K., Ghinassi, M. and Nemec, W. 2014. Reciprocal Changes In Foreset To Bottomset Facies In A Gilbert-Type Delta: Response To Short-Term Changes In Base Level. *Journal of Sedimentary Research*. 84(11), pp.1079–1095.

Gastaldo, R.A and Huc, A-Y. 1992. Sediment Facies, Depositional Environments, and Distribution of Phytoclasts in the Recent Mahakam River Delta, Kalimantan, Indonesia. *Palaios*. 7(6) pp. 574-590.

Gradstein, F.M., Anthonissen, E., Brunstad,H., Charnock, M., Hammer, O., Hellem, T., Lervik, K.S., Norwegian offshore Stratigraphic Lexicon (NORLEX). 2010 *Newsletters on Stratigraphy* 44. pp73-86

Gradstein, F. 2017. Lundin Norway lithostratigraphic charts. Available online at https://timescalefoundation.org/resources/NW_Europe_Lex/stratchart.php

Grunnaleite, I. and Gabrielsen, R.H. 1995. Structure of the Møre basin, mid-Norway continental margin. *Tectonophysics*. 252(1), pp.221–251.

Halland, E.K., Bjørnestad, A., Magnus, C., Riis, F., Meling, I.M., Gjeldvik, I.T., Tappel, I.M., Mujezinović, J., Bjørheim, M., Rød, R.S. and Pham, V.T.H. 2014. 5. The Norwegian Sea *In: CO_2 Storage Atlas: Norwegian Continental Shelf. Stavanger, Norway:* Norwegian Petroleum Directorate (NPD), pp.75–105.

Henstra, G.A., Gawthorpe, R.L., Helland-Hansen, W., Ravnås, R. and Rotevatn, A. 2017. Depositional systems in multiphase rifts: seismic case study from the Lofoten margin, Norway*. Basin Research.* 29(4), pp.447–469.

Hovius, N. 1996. Regular spacing of drainage outlets from linear mountain belts. *Basin Research*. 8 (1). pp 29-44

Jackson, C.A.L., Gawthorpe, R.L., Carr, I.D., Sharp, I.R. 2005. Normal faulting as a control on the stratigraphic development of shallow marine syn-rift sequences: the Nukhul and Lower Rudeis Formations, Hammam Faraun fault block, Suez Rift, Egypt. *Sedimentology*. 52. pp. 313-338.

Johnson. P.W and Hansen, K. 1987. Method for Calibrating Stacking Velocities for Use in Time-Depth Conversion. *19th Annual Offshore Technology Conference.* Houston, Texas, April 27-30.

Jones, G.E.D., Welbon, A.I.F., Mohammadlou, H., Sakharov, A., Ford, J., Needham, T. and Ottesen, C. 2021. Complex stratigraphic fill of a small, confined syn-rift basins: an Upper Jurassic example from offshore mid-Norway *In:* D. Chiarella, S. G. Archer, J. A. Howell, C. A. L. Jackson, H. Kombrink and S. Patruno, eds. *Cross-Border Themes in Petroleum Geology II: Atlantic Margin and Barents Sea Geological Society Special Publication No. 495*: Geological Society of London.

Jongepier, K., Rui, J.C. and Grue, K. 1996. Triassic to Early Cretaceous stratigraphic and structural development of the northeastern Møre Basin margin, off Mid-Norway. *Norsk Geologisk Tidsskrift.*, p.17.

Leeder, M.R. and Jackson, J.A. 1993. The interaction between normal faulting and drainage in active extensional basins, with examples from the western United States and central Greece. *Basin Research.* 5(2), pp.79–102.

Leeder, M.R., Portman, C., Andrews, J.E., Collier, R.E.Ll., Finch, E., Gawthorpe, R.L., McNeill, L.C., Pérez-Arlucea, M. and Rowe, P. 2005. Normal faulting and crustal deformation, Alkyonides Gulf and Perachora Peninsula, eastern Gulf of Corinth rift, Greece. *Journal of the Geological Society.* 162(3), pp.549–561.

Marsden, D. 1989. Layer cake depth conversion, Part I. *The Leading Edge*. 8. 10-14.

Martinius, A.W., Kaas, I., Næss, A., Helgesen, G., Kjærefjord, J.M. and Leith, D.A. 2001. Sedimentology of the heterolithic and tide-dominated tilje formation (Early Jurassic, Halten Terrace, Offshore Mid-Norway) *In:* O. J. Martinsen and T. Dreyer, eds. *Sedimentary Environments Offshore Norway — Palaeozoic to Recent Norwegian Petroleum Society Special Publications* pp.103–144.

Massari F., Colella A. 1988. Evolution and types of fan-delta systems in some major tectonic settings. *In* Nemec W., Steel R.J. (Eds.), *Fan Deltas: Sedimentology and Tectonic Settings*, Blackie, Glasgow pp. 103-122

Mjelde, R., Faleide, J.I., Breivik, A.J. and Raum, T. 2009. Lower crustal composition and crustal lineaments on the Vøring Margin, NE Atlantic: A review. *Tectonophysics*. 472(1), pp.183–193.

Mørk, M.B.E. and Johnsen, S.O. 2005. Jurassic sandstone provenance and basement erosion in the Møre margin – Froan Basin area. *NGU Bulletin*. 443, p.14.

Morley, C.K. and Lambiase, J.J. 1995. Developments in the structural geology of rifts over the last decade and their impact on hydrocarbon exploration *In* Lambiase, J.J eds. *Hydrocarbon Habitat in Rift Basins, Geological Society Special Publication No. 80.* Geological Society of London, pp.1–32.

Muñoz-Barrera, J.M., Rotevatn, A., Gawthorpe, R.L., Henstra, G.A. and Kristensen, T.B. 2020. The role of structural inheritance in the development of high-displacement crustal faults in the necking domain of rifted margins: The Klakk Fault Complex, Frøya High, offshore mid-Norway. *Journal of Structural Geology.* 140, p.104163.

Muñoz-Barrera, J. M., Rotevatn, A., Gawthorpe, R.L., Henstra, G., & Kristensen, T. B. 2022. Supradetachment basins in necking domains of rifted margins: Insights from the Norwegian Sea. *Basin Research*, 34, 991– 1019. https://doi.org/10.1111/bre.12648

Muravchik, M., Gawthorpe, R.L., Sharp, I.R., Rarity, F. and Hodgetts, D. 2018. Sedimentary environment evolution in a marine hangingwall dip slope setting. El Qaa Fault Block, Suez Rift, Egypt. *Basin Research*. 30(S1), pp.452–478.

Mutterlose, J., Brumsack, H., Flögel, S., Hay, W., Klein, C., Langrock, U., Lipinski, M., Ricken, W., Söding, E., Stein, R. and Swientek, O. 2003. The Greenland-Norwegian Seaway: A key area for understanding Late Jurassic to Early Cretaceous paleoenvironments. *Paleoceanography*. 18(1).

Nemec, W. 1990. Aspects of Sediment Movement on Steep Delta Slopes *In:* A. Colella and D. B. Prior, eds. *Coarse-Grained Deltas*. John Wiley & Sons, Ltd, pp.29–73.

Nielsen, L.H. and Johannessen, P.N. 2009. Facies architecture and depositional processes of the Holocene–Recent accretionary forced regressive Skagen spit system, Denmark. *Sedimentology*. 56(4), pp.935–968.

Nøttvedt, A., Berge, A.M., Dawers, N.H., Færseth, R.B., Häger, K.O., Mangerud, G. and Puigdefabregas, C. 2000. Syn-rift evolution and resulting play models in the Snorre-H area, northern North Sea *In:* A Nøttvedt, B. T. Larsen, R. H. Gabrielsen, S. Olaussen, H. Brekke, B. Tørudbakken, Ø. Birkeland and J. Skogseid, eds. *Dynamics of the Norwegian Margin, Geological Society, London, Special Publication No. 167*. Geological Society of London, pp.179–218.

Nyberg, B., Helland-Hansen, W., Gawthorpe, R., Tillmans, F. and Sandbakken, P. 2021. Assessing first-order BQART estimates for ancient source-to-sink mass budget calculations. *Basin Research.* 33(4), pp.2435–2452.

Olesen, O., Brönner, M., Ebbing, J., Gellein, J., Gernigon, L., Koziel, J., Lauritsen, T., Myklebust, R., Pascal, C., Sand, M., Solheim, D. and Usov, S. 2010. New aeromagnetic and gravity compilations from Norway and adjacent areas: methods and applications. *Geological Society, London, Petroleum Geology Conference series.* 7(1), pp.559–586.

Osmundsen, P.T. and Ebbing, J. 2008. Styles of extension offshore mid-Norway and implications for mechanisms of crustal thinning at passive margins. *Tectonics.* 27(6).

Osmundsen, P.T. and Péron-Pinvidic, G. 2018. Crustal-Scale Fault Interaction at Rifted Margins and the Formation of Domain-Bounding Breakaway Complexes: Insights From Offshore Norway. *Tectonics.* 37(3), pp.935–964.

Osmundsen, P.T., Péron-Pinvidic, G., Ebbing, J., Erratt, D., Fjellanger, E., Bergslien, D. and Syvertsen, S.E. 2016. Extension, hyperextension and mantle exhumation offshore Norway: a discussion based on 6 crustal transects. *Norwegian Journal of Geology*. Pp. 343-372

Gernigon, L., Franke, D., Geoffroy, L., Schiffer, C., Foulger, G.R. and Stoker, M. 2020. Crustal fragmentation, magmatism, and the diachronous opening of the Norwegian-Greenland Sea. *Earth-Science Reviews*. **206**, p.102839.

Patruno, S., Hampson, G.J., Jackson, C.A-L. 2015. Quantitative characterisation of deltaic and subaqueous clinoforms. *Earth-Science Reviews*. 142. pp 79-119

Pechlivanidou, S., Cowie, P.A., Duclaux, G., Nixon, C.W., Gawthorpe, R.L. and Salles, T. 2019. Tipping the balance: Shifts in sediment production in an active rift setting. *Geology*. **47**(3), pp.259–262.

Peron-Pinvidic, G., Manatschal, G. and Osmundsen, P.T. 2013. Structural comparison of archetypal Atlantic rifted margins: A review of observations and concepts. *Marine and Petroleum Geology*. 43, pp.21–47.

Postma, G. 1984. Slumps and their deposits in fan delta front and slope. *Geology*. 12(1), pp.27–30.

Prior, D.B. and Bornhold, B.D. 1989. Submarine sedimentation on a developing Holocene fan delta. *Sedimentology.* 36(6), pp.1053–1076.

Privat, A.M.-L.J., Hodgson, D.M., Jackson, C.A.-L., Schwarz, E. and Peakall, J.2021. Evolution from syn-rift carbonates to early post-rift deep-marine intraslope lobes: The role of rift basin physiography on sedimentation patterns. Sedimentology. *Online*

Rapozo, B.F., Córdoba, V.C. and Antunes, A.F. 2021. Tectono-stratigraphic evolution of a cretaceous intracontinental rift: Example from Rio do Peixe Basin, north-eastern Brazil. *Marine and Petroleum Geology.* 126, p.104899.

Ravnås, R., Bondevik., K., Helland-Hansen, W., Lømo, L., Ryseth,A and Steel, R.J. 1997. Sedimentation history as an indicator of rift initiation and development: the Late Bajocian-Bathonian evolution of the Oseberg-Brage area, northern North Sea. *Norsk Geologisk Tidsskrift*. 77. pp 205-232.

Ravnås, R. and Steel, R.J. 1998. Architecture of Marine Rift-Basin Successions. *AAPG Bulletin*. 82(1), pp.110–146.

Roberts, A.M., Corfield, R.I., Kusznir, N.J., Matthews, S.J., Hansen, E.-K. and Hooper, R.J. 2009. Mapping palaeostructure and palaeobathymetry along the Norwegian Atlantic continental margin: Møre and Vøring basins. *Petroleum Geoscience.* 15(1), pp.27–43.

Rohais, S., Eschard, R. and Guillocheau, F. 2008. Depositional model and stratigraphic architecture of rift climax Gilbert-type fan deltas (Gulf of Corinth, Greece). *Sedimentary Geology*. 210(3), pp.132–145.

Romans, B.W., Castelltort, S., Covault, J.A., Fildani, A. and Walsh, J.P. 2016. Environmental signal propagation in sedimentary systems across timescales. *Earth-Science Reviews.* 153, pp.7–29.

Rossi, V.M. and Steel, R.J. 2016. The role of tidal, wave and river currents in the evolution of mixed-energy deltas: Example from the Lajas Formation (Argentina). *Sedimentology.* 63(4), pp.824–864.

Rubi, R., Rohais, S., Bourquin, S., Moretti, I. and Desaubliaux, G. 2018. Processes and typology in Gilbert-type delta bottomset deposits based on outcrop examples in the Corinth Rift. *Marine and Petroleum Geology*. 92, pp.193–212.

Skarbø, O., Bakke, S., Jacobsen, T., Krokstad, W., Lundschien, B., Myhr, M.B., Rise, L., Schou, L., Smelror, M., Verdenius, J.G., Vigran, J.O. & Århus, N. (1988) Shallow Drilling Off Møre-Trøndelag 1998, IKU Sintef group, 387.

Smyrak-Sikora, A., Nicolaisen, J.B., Braathen, A., Johannessen, E.P., Olaussen, S. and Stemmerik, L. 2021. Impact of growth faults on mixed siliciclastic-carbonate-evaporite deposits during rift climax and reorganisation—Billefjorden Trough, Svalbard, Norway. Basin Research. *Accepted Version Online*

Smyrak-Sikora, A., Johannessen, E.P., Olaussen, S., Sandal, G. and Braathen, A. 2018. Sedimentary architecture during Carboniferous rift initiation – the arid Billefjorden Trough, Svalbard. *Journal of the Geological Society*. **176**(2), pp.225–252.

Sømme, T.O., Helland-Hansen, W., Martinsen, O.J. and Thurmond, J.B. 2009. Relationships between morphological and sedimentological parameters in source-to-sink systems: a basis for predicting semi-quantitative characteristics in subsurface systems. *Basin Research.* 21(4), pp.361–387.

Sømme, T.O., Jackson, C.A.L., Lunt, I., Martinsen, O. 2010. Source-to-Sink in Rift Basins – Prediciting Reservoir Distribution in Ancient, Subsurface Systems. *American Association of Petroleum Geologists Annual Convention and Exhibition, New Orleans, Louisana, USA, April 11-14 2010. Search and Discovery article #10258.*

Statoil, 1994. Completion Report Well 6306/6-1 PL198 Harstad, Norway: Statoil. Available from: https://factpages.npd.no/pbl/wellbore_documents/2384_6306_6_1_COMPLETION_REPORT_AND_LOG.pdf.

Talling, P.J., Stewart, M.D., Stark, C.P., Gupta, S., Vincent, S.J. 1997. Regular spacing of drainage outlets from linear fault blocks. *Basin Research* 9. pp 275-302.

Van der Zwaan, C.J. 1990: Palynostratigraphy and Palynofacies Reconstruction of the Upper Jurassic to Lowermost Cretaceous of the Draugen Field, Offshore Mid Norway. Reviews of Palaeobotany and Palynology 62, 157-186Wilson, P., Elliott, G.M., Gawthorpe, R.L., Jackson, C.A.-L., Michelsen, L. and Sharp, I.R. 2015. Lateral variation in structural style along an evaporite-influenced rift fault system in the Halten Terrace, Norway: Influence of basement structure and evaporite facies. *Journal of Structural Geology.* 79, pp.110–123.

Wilson, P., Elliott, G.M., Gawthorpe, R.L., Jackson, C.A.-L., Michelsen, L. and Sharp, I.R. 2015. Lateral variation in structural style along an evaporite-influenced rift fault system in the Halten Terrace, Norway: Influence of basement structure and evaporite facies. *Journal of Structural Geology*. **79**, pp.110–123..

Figure 1: A) Regional map of the key structural elements of the Norwegian Continental shelf offshore Mid-Norway , After NPD (2022). SR – Sklinna Ridge, VFC – Vingleia Fault Complex, BFC – Bremmstein Fault Complex. FF – Froan Fault B) Regional 2D seismic cross-section showing the location of the Frøya High bound a high-displacement normal fault – the Klakk Fault Complex within the necking domain of the Norwegian margin in this region. C) Inset of Frøya High regional section highlighting the studied stratigraphy in the footwall of the Klakk Fault Complex.

Figure 2: A) Well-to-seismic tie for the stratigraphic interval of interest. A synthetic seismogram is generated from the sonic and density logs of well 6306/6-1 (Location in Figure 1, 3). Key surfaces that are recognised in the well are thus linked to their corresponding reflector in the seismic reflection survey shown in **(B). C)** Stratigraphic chart highlighting the lithostratigraphic nomenclature for the Norwegian Margin in the Southern Norwegian Sea (modified from Gradstein et al., 2010 and Gradstein, 2017). ¨TVD – True Vertical Depth, TWT – Two-Way Time, FH- Frøya High, SR – Sklinna Ridge, GH – Gossa High. Tectonic events summarised from Bunkholt et al. (2022).

Figure 3: TWT structure maps of the three key surfaces; **A**) Top Basement, **B**) Base Viking Group and **C)** Top Viking Group (BCU)) used in this study for isopachs and depositional system reconstruction. Ticks on onlap extent lines point downdip towards deeper onlap.

Figure 4: Uninterpreted (A) and Interpreted (B) NW-SE trending seismic line intersecting Area A, E and F highlighting the character of the Top Viking/BCU surface and Viking and Cromer Knoll Group character in the area. Key truncation relationships are marked with arrows highlighting downlap within the Viking Group in Area A, Onlap of the Cromer Knoll Group in Area F, and truncation of the Middle Jurassic and Mesozoic stratigraphy by the Base Viking Group surface. Location and Areas are demonstrated in Figure 4.

Figure 5: Isopach maps of A) Late Jurassic, Viking Group, generated by depth-converting and combining the base and top Viking Group TWT structure maps shown in Figures 3b and 3c, respectively. B) Early Cretaceous, Cromer Knoll Group, generated by depth converting and combining the top Viking Group TWT structure map (Figure. 3c) and an autotracked TWT surface of the base Shetland Group reflector. Key depocenters referred to in the text are labelled A, B, C, O – G.

Figure 6: Uninterpreted (A) and interpreted (B)detailed seismic image of Viking Gp. wedge B intersection with well 6306/9-1 (Figure. 5a). Location shown in Figure 4. K – Cretaceous. J – Jurassic. Log within 6306/9-1 is provided in Figure 9. Yellow dots relate to the Top and Base of the Rogn Formation. Seismic sections are plotted in time and are not flattened to preserve the the true well path and allow the well log to be anchored on Top Viking and Top Basement reflectors.

Figure 7: Non-flattened and Top Shetland Group flattened seismic sections through thickness anomalies of The Viking Group termed wedges B, C and C. All lines are west - left and east - right. A) Seismic line (unflattened and falttened) through Wedge A. B) Inset location map of cropped Viking Group thickness map, with seismic line locations (red lines). C) Seismic line (unflattened and flattened) through wedge C. D) Seismic line (unflattened and flattened) intersecting with 6306/6-1 through depocentre D. Erosional feature relates to Depocentre E in Figure 5b.

Figure 8: Uninterpreted (A) and Interpreted (B) composite, approximately N-S oriented seismic lines with the three Viking Group wedges labelled. C, D) Insets of Wedge B and A respectively showing internal truncations and seismic character. Location shown in Figure 4.

Figure 9: Summary well log for the Late Jurassic stratigraphy of 6306/9-1 compiled from wireline, sidewall core, biostratigraphic and borehole imaging observations. FMI – Formation Microresistivity Image, UBI – Ultrasonic Borehole Imager.

Figure 10. A) Detail of Viking Group thickness map (Figure 4a) highlighting amphitheatre shaped depression bound by steep erosional scars within the eastern edge of Wedge A. Location on Figure 4. B) S (left) – N (right) oriented seismic line highlighting concave depressions within The Viking Group on the eastern edge of Wedge A. Location in part A.

Figure 11. Cross sections demonstrating a simple restoration of the Top Viking Group/BCU structure map. The surface of **Figure 4c** is depth converted and rotated so that the areas interpreted to represent horizontal topsets of the deltaic clinoform packages A, B C, and D (Figure 12). Location in Figure 1a.

Figure 12. Restored, depth converted, BCU structure map is based on rotation (Figure 11) to horizontal of the best-fit plane through the palaeo-horizontal topsets of the Upper Jurassic clinoform package. The resultant surface represents an approximation of the topography of the Frøya High at the end of the Jurassic. A-D – Deltaic clinoform packages. 1-4 – Deeply eroded areas.

Figure 13: Simplified and interpretive palaeogeographic maps based on the distribution of stratigraphic packages and depositional environments as interpreted in the present study A) Generalised palaeogeographic reconstruction of the south-eastern part of the Frøya High and Froan Basin during the Late Jurassic deposition of deltaic clinoform packages (A,B,C) fed by catchments eroding from Triassic-Middle Jurassic subcrop (a,b,c). **B)** Generalised palaeogeographic reconstruction of the south-eastern part of the Frøya High and Froan Basin during the Early Cretaceous, forming substantial erosional systems, redirected to the south, compared to the eastern-draining systems during the Late Jurassic.

Figure 14: A new, simple palaeogeographic model for the Late Jurassic deposition along the south-eastern margin of the Frøya High. The shoreline is supplied with abundant clastic material in the south, and potentially in the middle, and a longshore current connects it to the Draugen ridge that may represent a spit system rather than a detached sand ridge.

Figure 15: Conceptual cartoons for evolutionary models of dip slope shoreline systems in A) A footwall uplift driven dip slope shoreline system. Here, progressive uplift in the footwall of a major fault drives sediment flux (T1 – T2) but also induces headward erosion from other catchments which capture dip slope drainage (T3). B) A hangingwall subsidence driven dip slope shoreline systems. Here, progressive subsidence in the hangingwall of a major fault drives a structural gradient to produce drainage catchments which are gradually transgressed (T2) and recorded as protracted shutdowns of shoreline systems (T3).

FIGURE 1

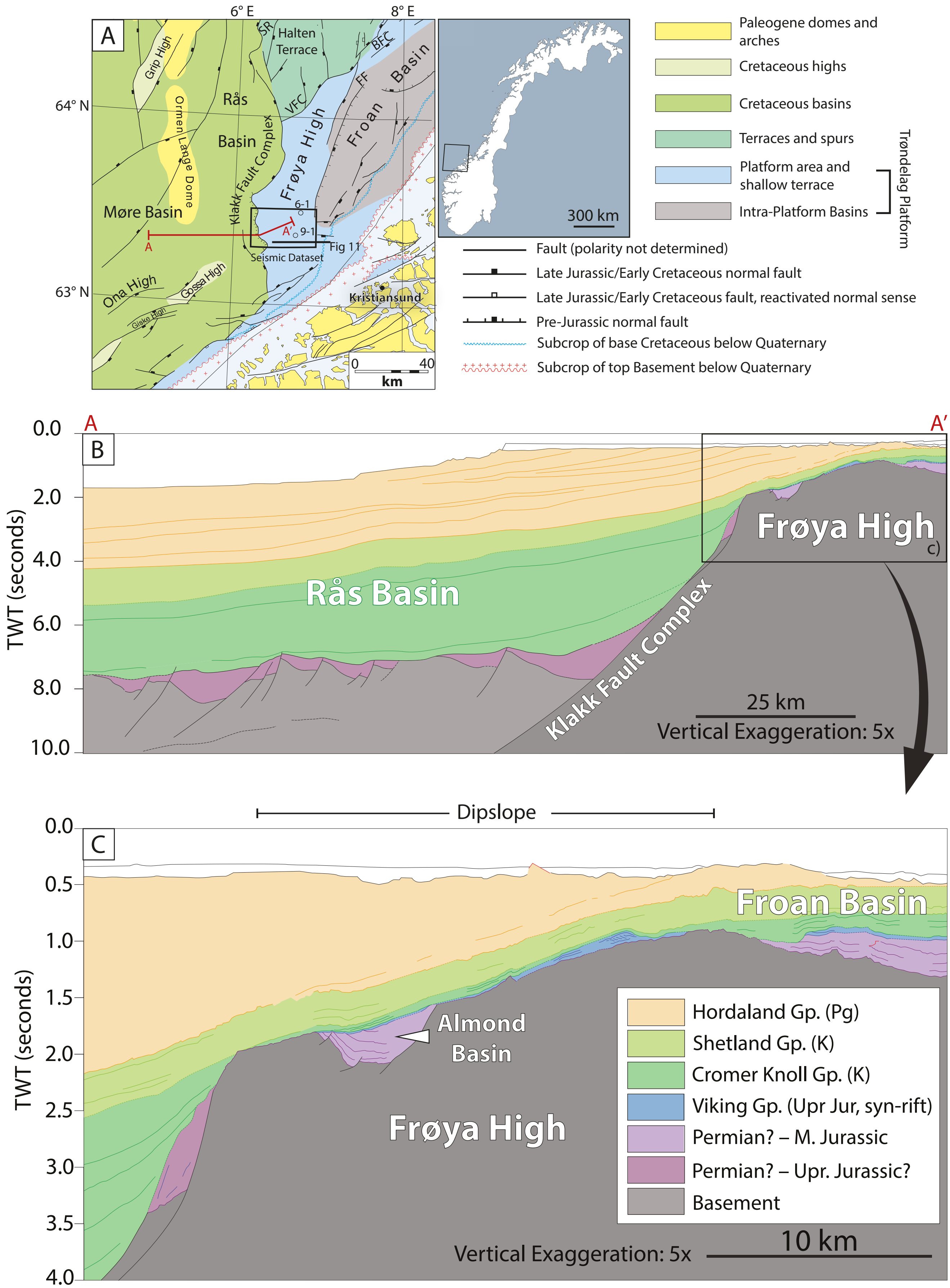

A
6° E
8° E
64° N
63° N
Grip High
Ormen Lange Dome
Rås Basin
Møre Basin
Klakk Fault Complex
SR
Halten Terrace
VFC
Frøya High
FF
BFC
Froan Basin
6-1
9-1
A
A′
Fig 11
Seismic Dataset
Ona High
Gossa High
Giske High
Kristiansund
0
40
km
300 km
Paleogene domes and arches
Cretaceous highs
Cretaceous basins
Terraces and spurs
Platform area and shallow terrace
Intra-Platform Basins
Trøndelag Platform
Fault (polarity not determined)
Late Jurassic/Early Cretaceous normal fault
Late Jurassic/Early Cretaceous fault, reactivated normal sense
Pre-Jurassic normal fault
Subcrop of base Cretaceous below Quaternary
Subcrop of top Basement below Quaternary
B
A
A′
0.0
2.0
4.0
6.0
8.0
10.0
TWT (seconds)
Rås Basin
Frøya High
c)
Klakk Fault Complex
25 km
Vertical Exaggeration: 5x
C
Dipslope
0.0
0.5
1.0
1.5
2.0
2.5
3.0
3.5
4.0
TWT (seconds)
Froan Basin
Almond Basin
Frøya High
Hordaland Gp. (Pg)
Shetland Gp. (K)
Cromer Knoll Gp. (K)
Viking Gp. (Upr Jur, syn-rift)
Permian? – M. Jurassic
Permian? – Upr. Jurassic?
Basement
Vertical Exaggeration: 5x
10 km

FIGURE 2

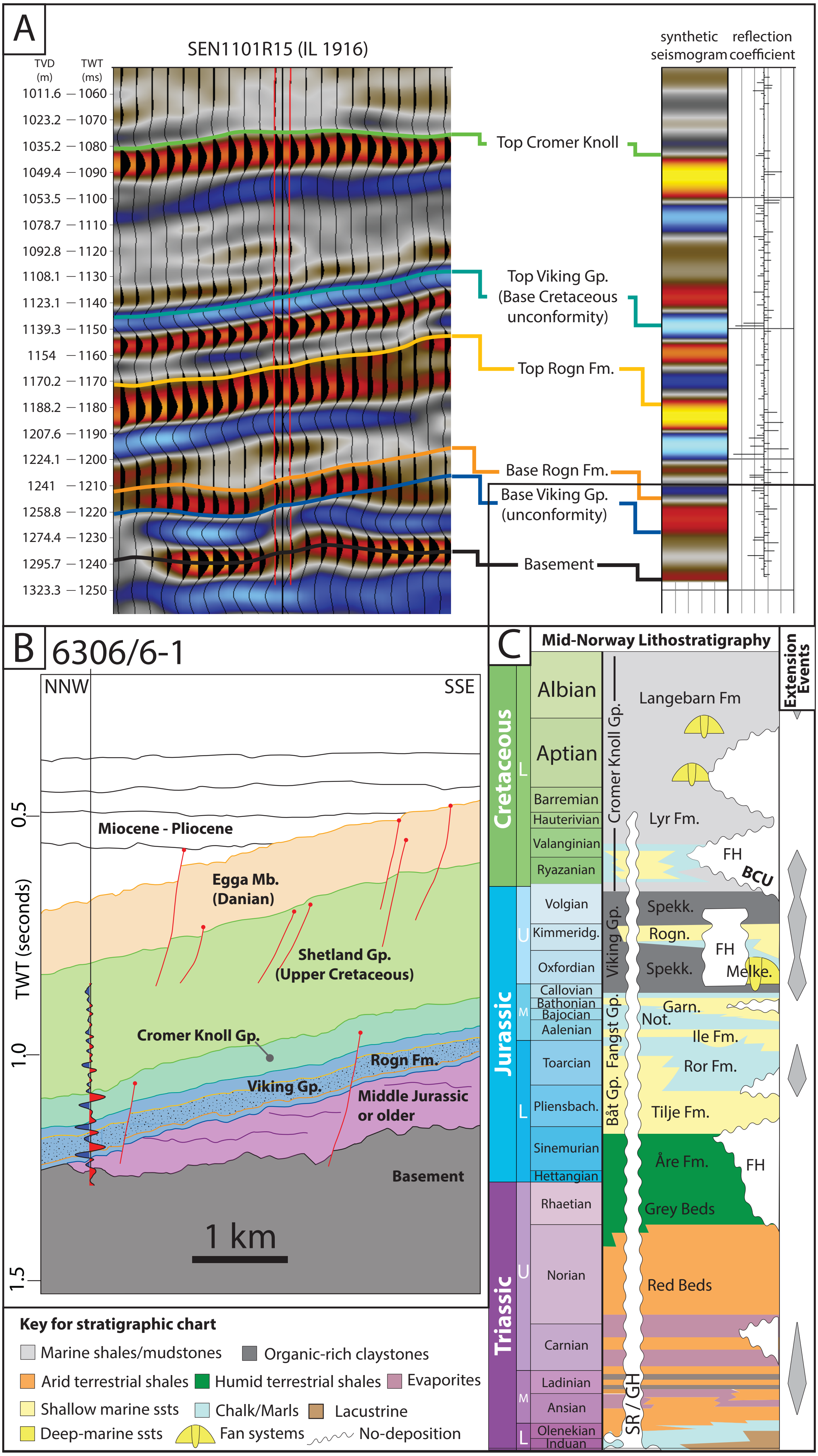

A
SEN1101R15 (IL 1916)
TVD (m)
TWT (ms)
synthetic seismogram
reflection coefficient
Top Cromer Knoll
Top Viking Gp. (Base Cretaceous unconformity)
Top Rogn Fm.
Base Rogn Fm.
Base Viking Gp. (unconformity)
Basement
B
6306/6-1
NNW
SSE
TWT (seconds)
Miocene - Pliocene
Egga Mb. (Danian)
Shetland Gp. (Upper Cretaceous)
Cromer Knoll Gp.
Rogn Fm.
Viking Gp.
Middle Jurassic or older
Basement
1 km
C
Mid-Norway Lithostratigraphy
Extension Events
Cretaceous
Jurassic
Triassic
Albian
Aptian
Barremian
Hauterivian
Valanginian
Ryazanian
Volgian
Kimmeridg.
Oxfordian
Callovian
Bathonian
Bajocian
Aalenian
Toarcian
Pliensbach.
Sinemurian
Hettangian
Rhaetian
Norian
Carnian
Ladinian
Ansian
Olenekian
Induan
Cromer Knoll Gp.
Viking Gp.
Fangst Gp.
Båt Gp.
SR / GH
Langebarn Fm
Lyr Fm.
FH
BCU
Spekk.
Rogn.
Spekk.
Melke.
Garn.
Not.
Ile Fm.
Ror Fm.
Tilje Fm.
Åre Fm.
Grey Beds
Red Beds
Key for stratigraphic chart
Marine shales/mudstones
Organic-rich claystones
Arid terrestrial shales
Humid terrestrial shales
Evaporites
Shallow marine ssts
Chalk/Marls
Lacustrine
Deep-marine ssts
Fan systems
No-deposition

FIGURE 3

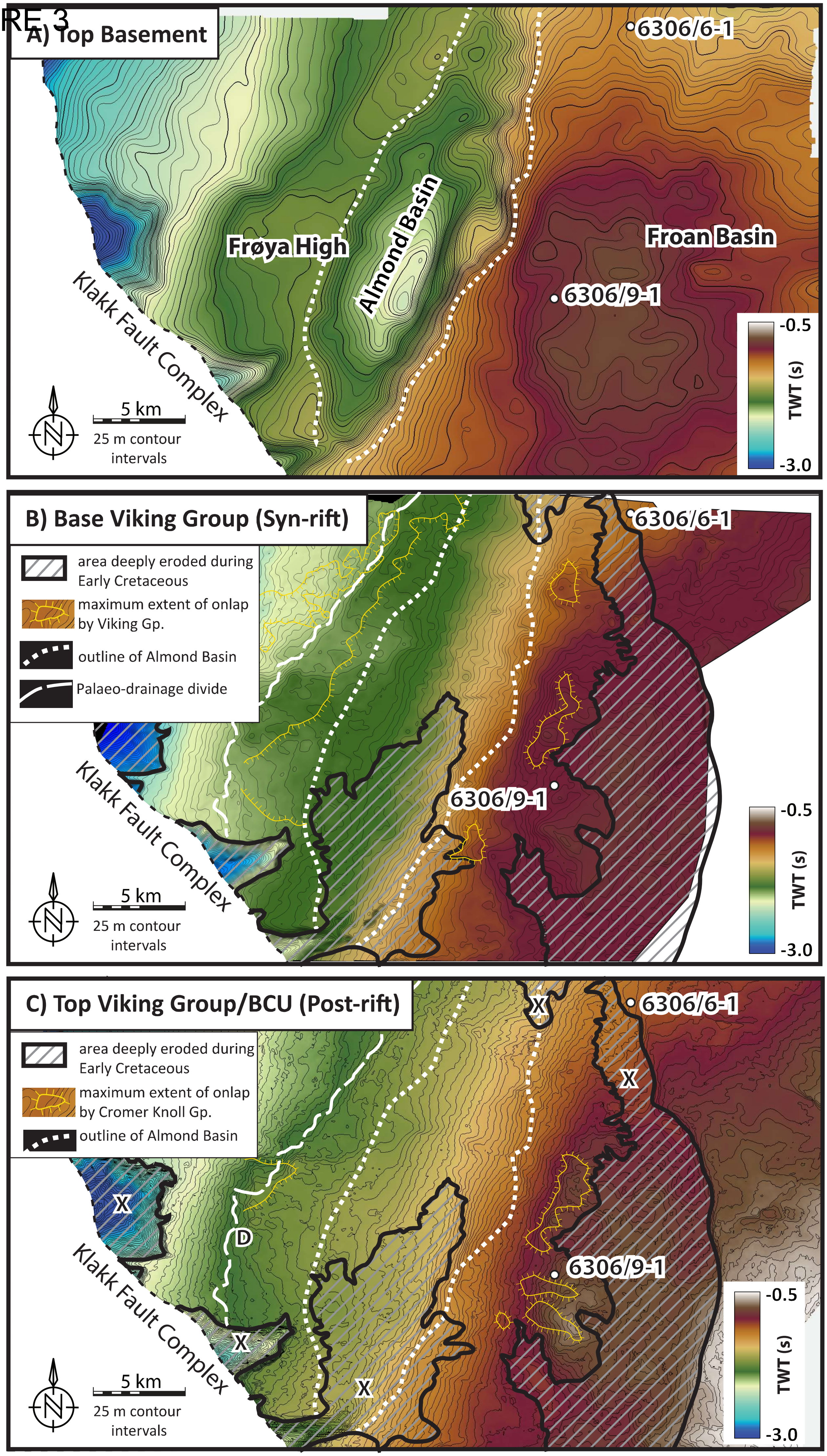

A) Top Basement
6306/6-1
Frøya High
Almond Basin
Froan Basin
6306/9-1
Klakk Fault Complex
5 km
25 m contour intervals
-0.5
TWT (s)
-3.0
B) Base Viking Group (Syn-rift)
area deeply eroded during Early Cretaceous
maximum extent of onlap by Viking Gp.
outline of Almond Basin
Palaeo-drainage divide
6306/6-1
6306/9-1
Klakk Fault Complex
5 km
25 m contour intervals
-0.5
TWT (s)
-3.0
C) Top Viking Group/BCU (Post-rift)
area deeply eroded during Early Cretaceous
maximum extent of onlap by Cromer Knoll Gp.
outline of Almond Basin
6306/6-1
6306/9-1
X
D
Klakk Fault Complex
5 km
25 m contour intervals
-0.5
TWT (s)
-3.0

FIGURE 4

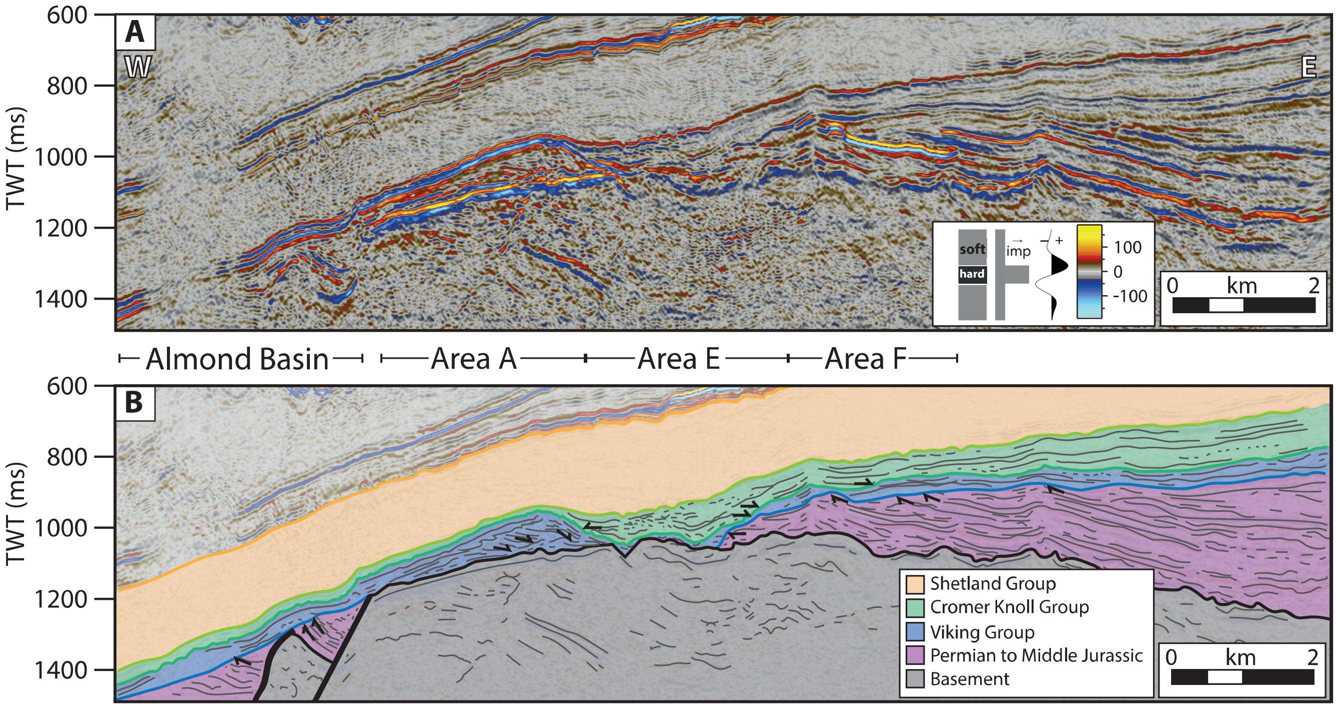
A
W
E
600
800
1000
1200
1400
TWT (ms)
soft
hard
imp
100
0
-100
0 km 2
Almond Basin
Area A
Area E
Area F
B
Shetland Group
Cromer Knoll Group
Viking Group
Permian to Middle Jurassic
Basement

FIGURE 5

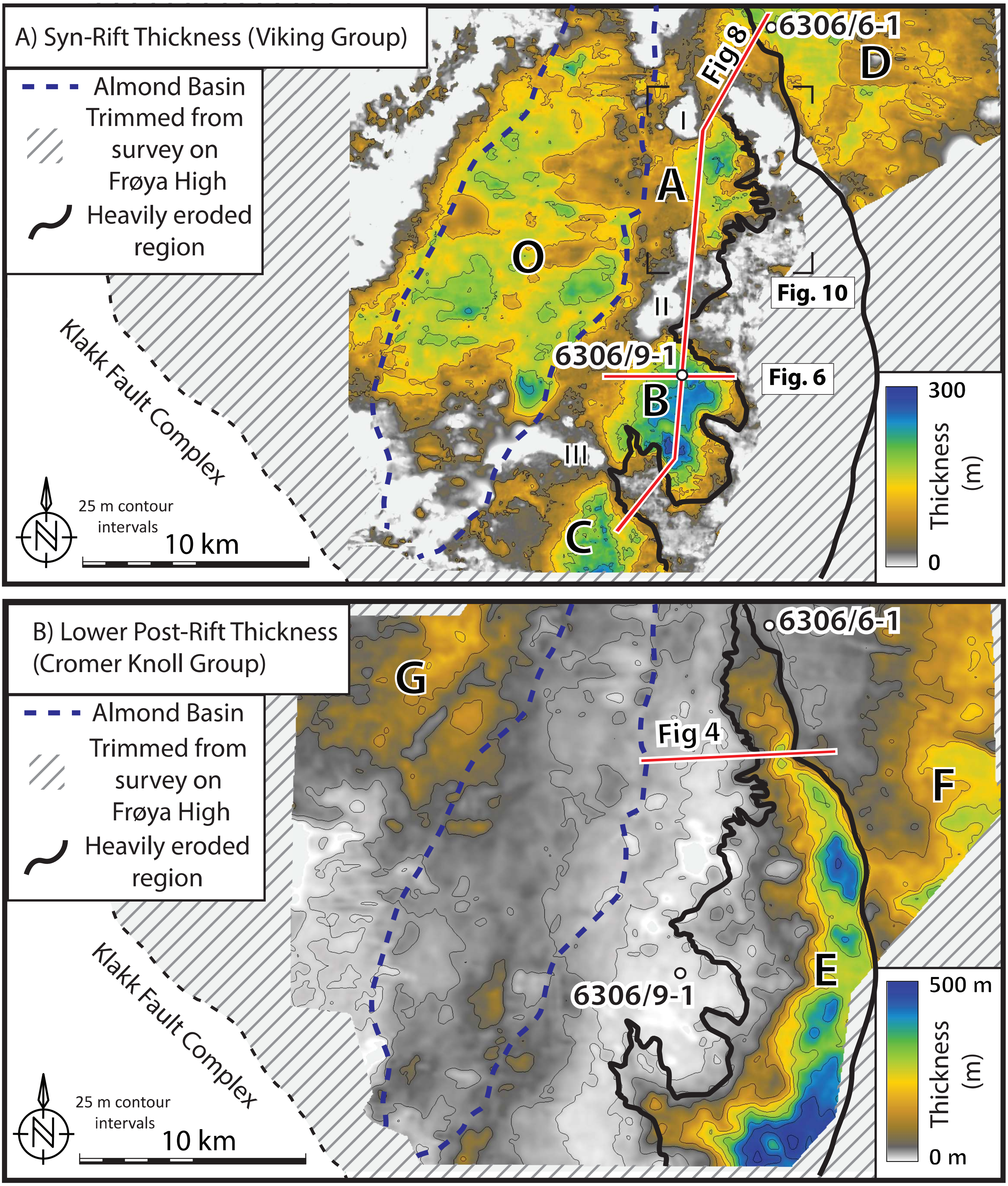

A) Syn-Rift Thickness (Viking Group)
Almond Basin
Trimmed from survey on Frøya High
Heavily eroded region
Klakk Fault Complex
25 m contour intervals
10 km
6306/6-1
Fig 8
D
I
A
O
Fig. 10
II
6306/9-1
Fig. 6
B
III
C
300
Thickness (m)
0
B) Lower Post-Rift Thickness (Cromer Knoll Group)
Almond Basin
Trimmed from survey on Frøya High
Heavily eroded region
Klakk Fault Complex
25 m contour intervals
10 km
6306/6-1
G
Fig 4
F
E
6306/9-1
500 m
Thickness (m)
0 m

FIGURE 6

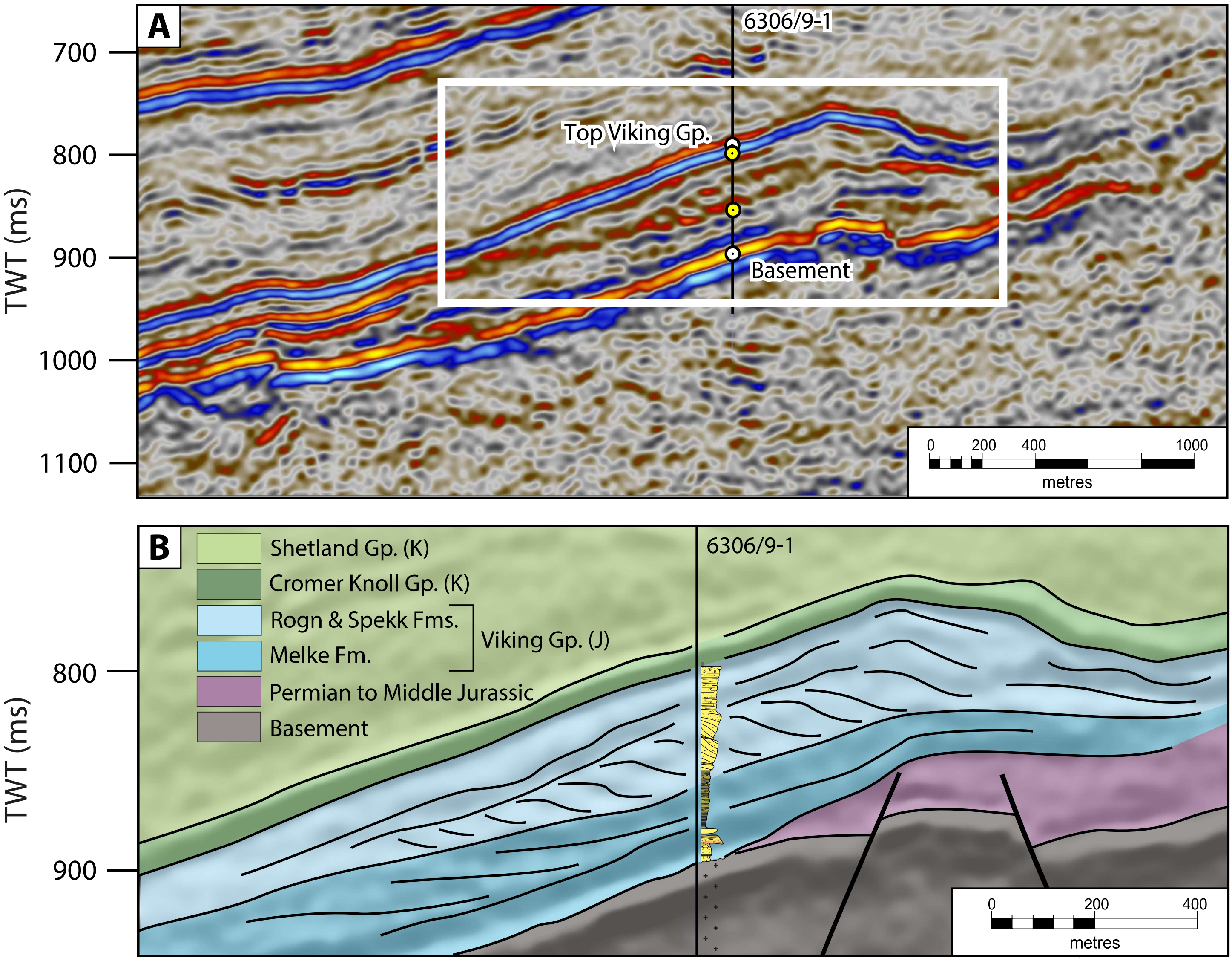
A
6306/9-1
Top Viking Gp.
Basement
TWT (ms)
700
800
900
1000
1100
0
200
400
1000
metres
B
Shetland Gp. (K)
Cromer Knoll Gp. (K)
Rogn & Spekk Fms.
Melke Fm.
Viking Gp. (J)
Permian to Middle Jurassic
Basement
6306/9-1
TWT (ms)
800
900
0
200
400
metres

FIGURE 7

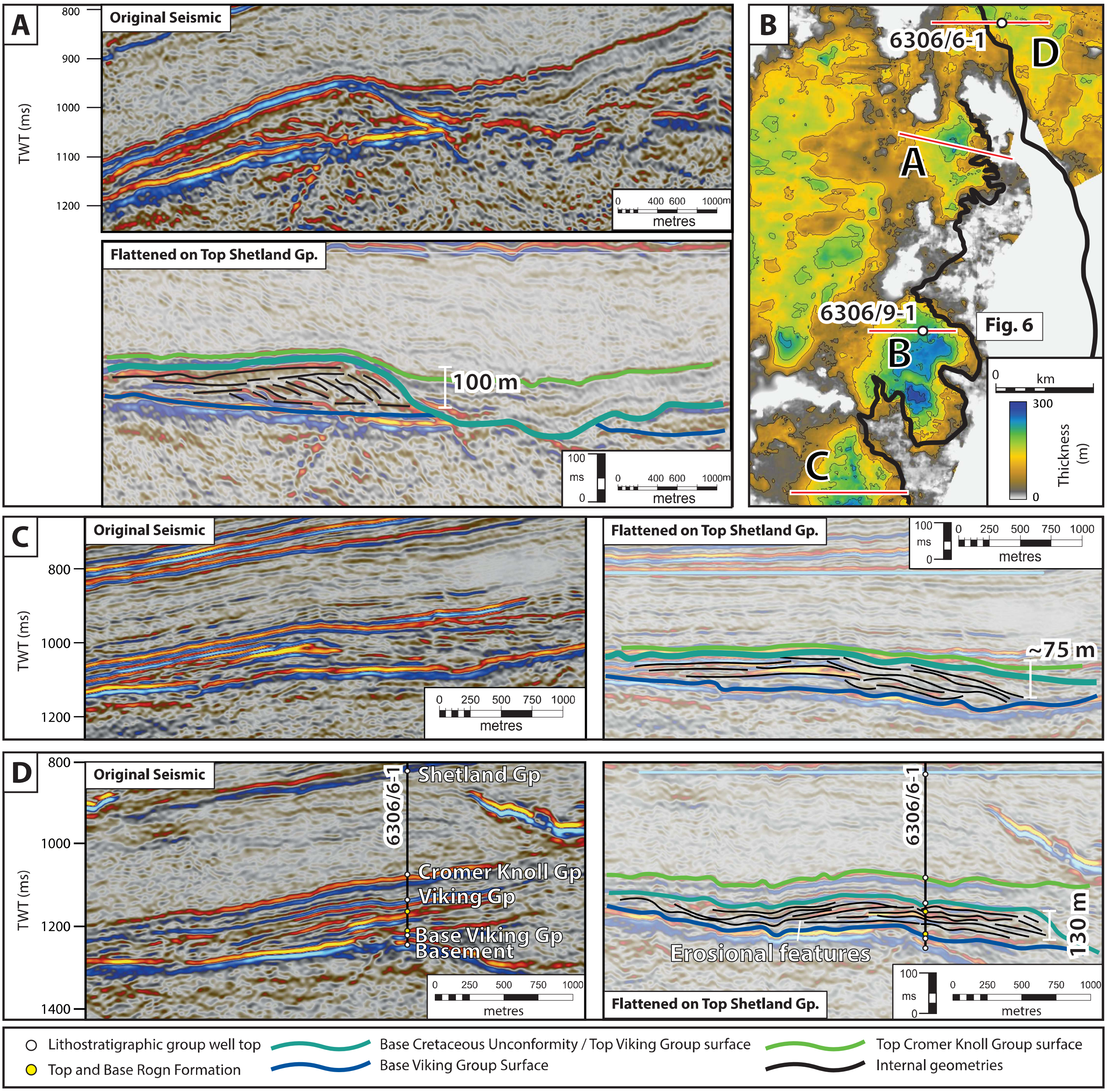

A
Original Seismic
TWT (ms)
800
900
1000
1100
1200
0 400 600 1000m
metres
Flattened on Top Shetland Gp.
100 m
100
ms
0
B
6306/6-1
D
A
6306/9-1
B
Fig. 6
C
0 km
300
Thickness (m)
0
C
Original Seismic
800
1000
1200
0 250 500 750 1000
metres
Flattened on Top Shetland Gp.
~75 m
D
Original Seismic
1400
6306/6-1
Shetland Gp
Cromer Knoll Gp
Viking Gp
Base Viking Gp
Basement
Erosional features
130 m
Lithostratigraphic group well top
Top and Base Rogn Formation
Base Cretaceous Unconformity / Top Viking Group surface
Base Viking Group Surface
Top Cromer Knoll Group surface
Internal geometries

FIGURE 8

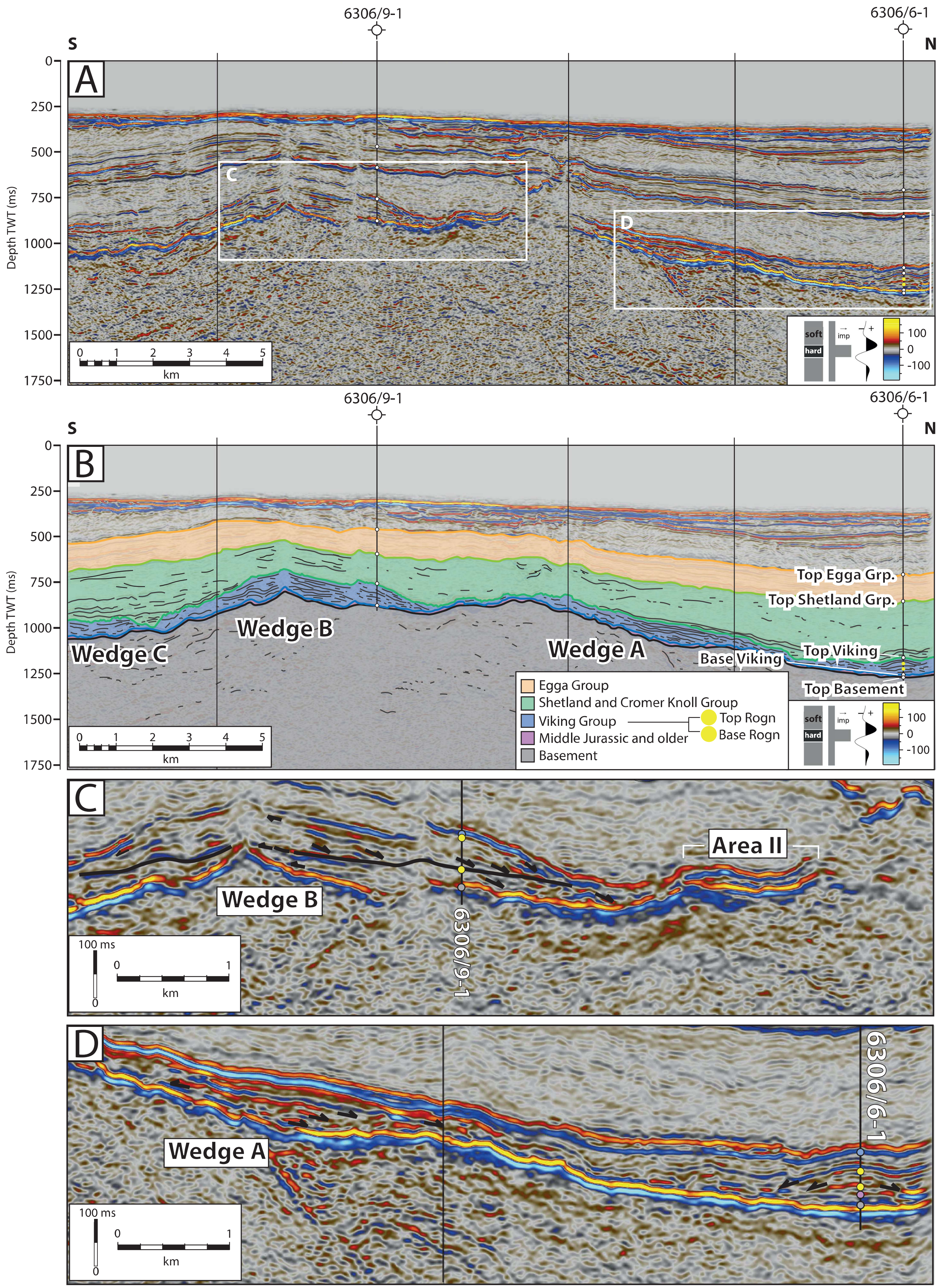

6306/9-1
6306/6-1
S
N
A
C
D
Depth TWT (ms)
0
250
500
750
1000
1250
1500
1750
0 1 2 3 4 5
km
soft
hard
imp
100
0
-100
B
Top Egga Grp.
Top Shetland Grp.
Top Viking
Base Viking
Top Basement
Wedge B
Wedge C
Wedge A
Egga Group
Shetland and Cromer Knoll Group
Viking Group
Middle Jurassic and older
Basement
Top Rogn
Base Rogn
Area II
100 ms
0 1
km

FIGURE 9

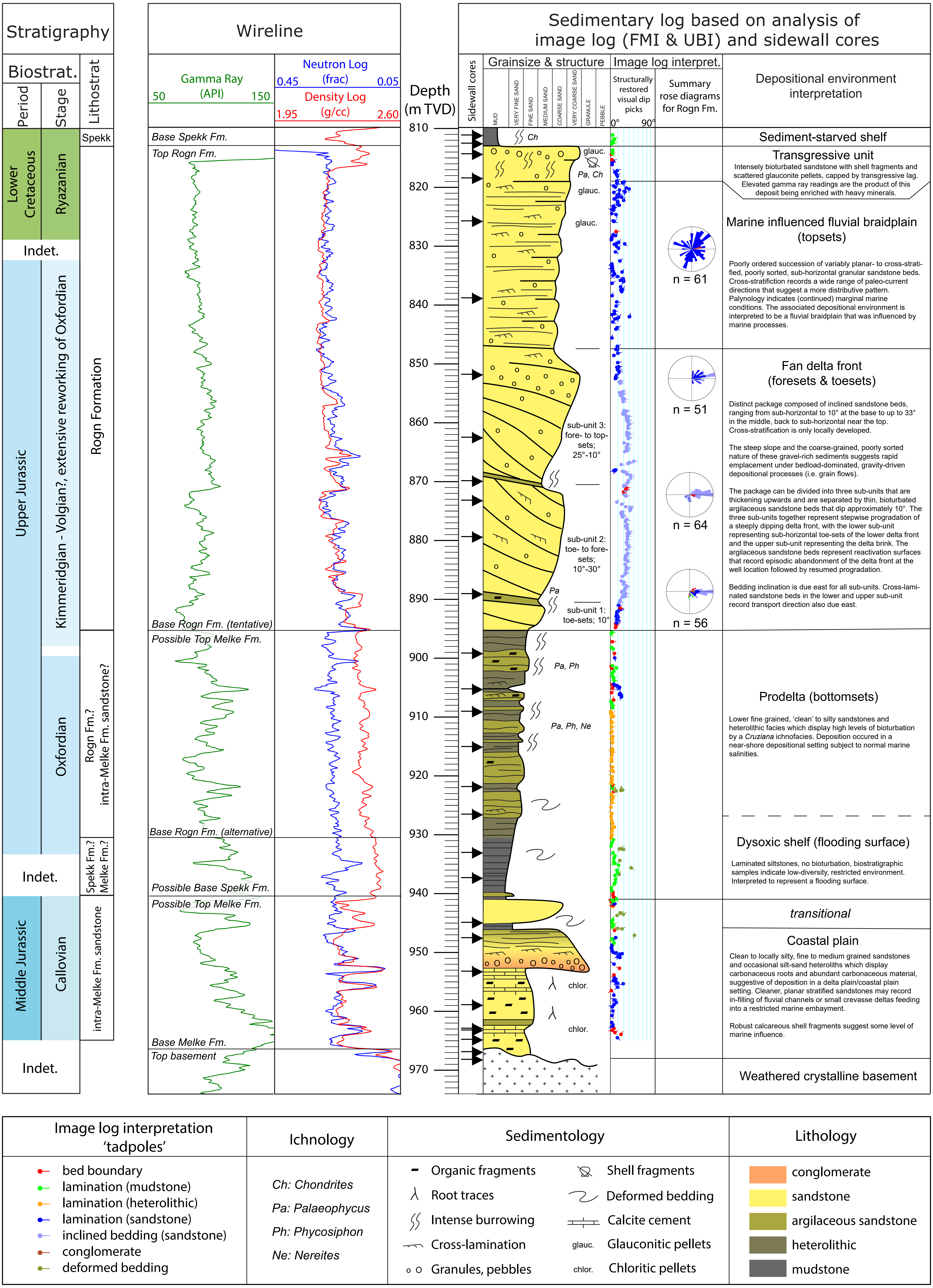

Stratigraphy
Biostrat.
Period
Stage
Lithostrat
Lower Cretaceous
Ryazanian
Spekk
Indet.
Upper Jurassic
Kimmeridgian - Volgian?, extensive reworking of Oxfordian
Rogn Formation
Oxfordian
Rogn Fm.? intra-Melke Fm. sandstone?
Spekk Fm.? Melke Fm.?
Indet.
Middle Jurassic
Callovian
intra-Melke Fm. sandstone
Indet.
Wireline
Gamma Ray (API)
50
150
Neutron Log (frac)
0.45
0.05
Density Log (g/cc)
1.95
2.60
Base Spekk Fm.
Top Rogn Fm.
Base Rogn Fm. (tentative)
Possible Top Melke Fm.
Base Rogn Fm. (alternative)
Possible Base Spekk Fm.
Possible Top Melke Fm.
Base Melke Fm.
Top basement
Depth (m TVD)
810
820
830
840
850
860
870
880
890
900
910
920
930
940
950
960
970
Sedimentary log based on analysis of image log (FMI & UBI) and sidewall cores
Sidewall cores
Grainsize & structure
MUD
VERY FINE SAND
FINE SAND
MEDIUM SAND
COARSE SAND
VERY COARSE SAND
GRANULE
PEBBLE
Ch
glauc.
Pa, Ch
glauc.
glauc.
sub-unit 3: fore- to top-sets; 25°-10°
sub-unit 2: toe- to fore-sets; 10°-30°
Pa
sub-unit 1: toe-sets; 10°
Pa, Ph
Pa, Ph, Ne
chlor.
chlor.
Image log interpret.
Structurally restored visual dip picks
0°
90°
Summary rose diagrams for Rogn Fm.
n = 61
n = 51
n = 64
n = 56
Depositional environment interpretation
Sediment-starved shelf
Transgressive unit
Intensely bioturbated sandstone with shell fragments and scattered glauconite pellets, capped by transgressive lag. Elevated gamma ray readings are the product of this deposit being enriched with heavy minerals.
Marine influenced fluvial braidplain (topsets)
Poorly ordered succession of variably planar- to cross-stratified, poorly sorted, sub-horizontal granular sandstone beds. Cross-stratification records a wide range of paleo-current directions that suggest a more distributive pattern. Palynology indicates (continued) marginal marine conditions. The associated depositional environment is interpreted to be a fluvial braidplain that was influenced by marine processes.
Fan delta front (foresets & toesets)
Distinct package composed of inclined sandstone beds, ranging from sub-horizontal to 10° at the base to up to 33° in the middle, back to sub-horizontal near the top. Cross-stratification is only locally developed.
The steep slope and the coarse-grained, poorly sorted nature of these gravel-rich sandstones suggests rapid emplacement under bedload-dominated, gravity-driven depositional processes (i.e. grain flows).
The package can be divided into three sub-units that are thickening upwards and are separated by thin, bioturbated argilaceous sandstone beds that dip approximately 10°. The three sub-units together represent stepwise progradation of a steeply dipping delta front, with the lower sub-unit representing sub-horizontal toe-sets of the lower delta front and the upper sub-unit representing the delta brink. The argilaceous sandstone beds represent reactivation surfaces that record episodic abandonment of the delta front at the well location followed by resumed progradation.
Bedding inclination is due east for all sub-units. Cross-laminated sandstone beds in the lower and upper sub-unit record transport direction also due east.
Prodelta (bottomsets)
Lower fine grained, 'clean' to silty sandstones and heterolithic facies which display high levels of bioturbation by a *Cruziana* ichnofacies. Deposition occured in a near-shore depositional setting subject to normal marine salinities.
Dysoxic shelf (flooding surface)
Laminated siltstones, no bioturbation, biostratigraphic samples indicate low-diversity, restricted environment. Interpreted to represent a flooding surface.
transitional
Coastal plain
Clean to locally silty, fine to medium grained sandstones and occasional silt-sand heteroliths which display carbonaceous roots and abundant carbonaceous material, suggestive of deposition in a delta plain/coastal plain setting. Cleaner, planar stratified sandstones may record in-filling of fluvial channels or small crevasse deltas feeding into a restricted marine embayment.
Robust calcareous shell fragments suggest some level of marine influence.
Weathered crystalline basement
Image log interpretation 'tadpoles'
bed boundary
lamination (mudstone)
lamination (heterolithic)
lamination (sandstone)
inclined bedding (sandstone)
conglomerate
deformed bedding
Ichnology
Ch: Chondrites
Pa: Palaeophycus
Ph: Phycosiphon
Ne: Nereites
Sedimentology
Organic fragments
Root traces
Intense burrowing
Cross-lamination
Granules, pebbles
Shell fragments
Deformed bedding
Calcite cement
glauc. Glauconitic pellets
chlor. Chloritic pellets
Lithology
conglomerate
sandstone
argilaceous sandstone
heterolithic
mudstone

FIGURE 10

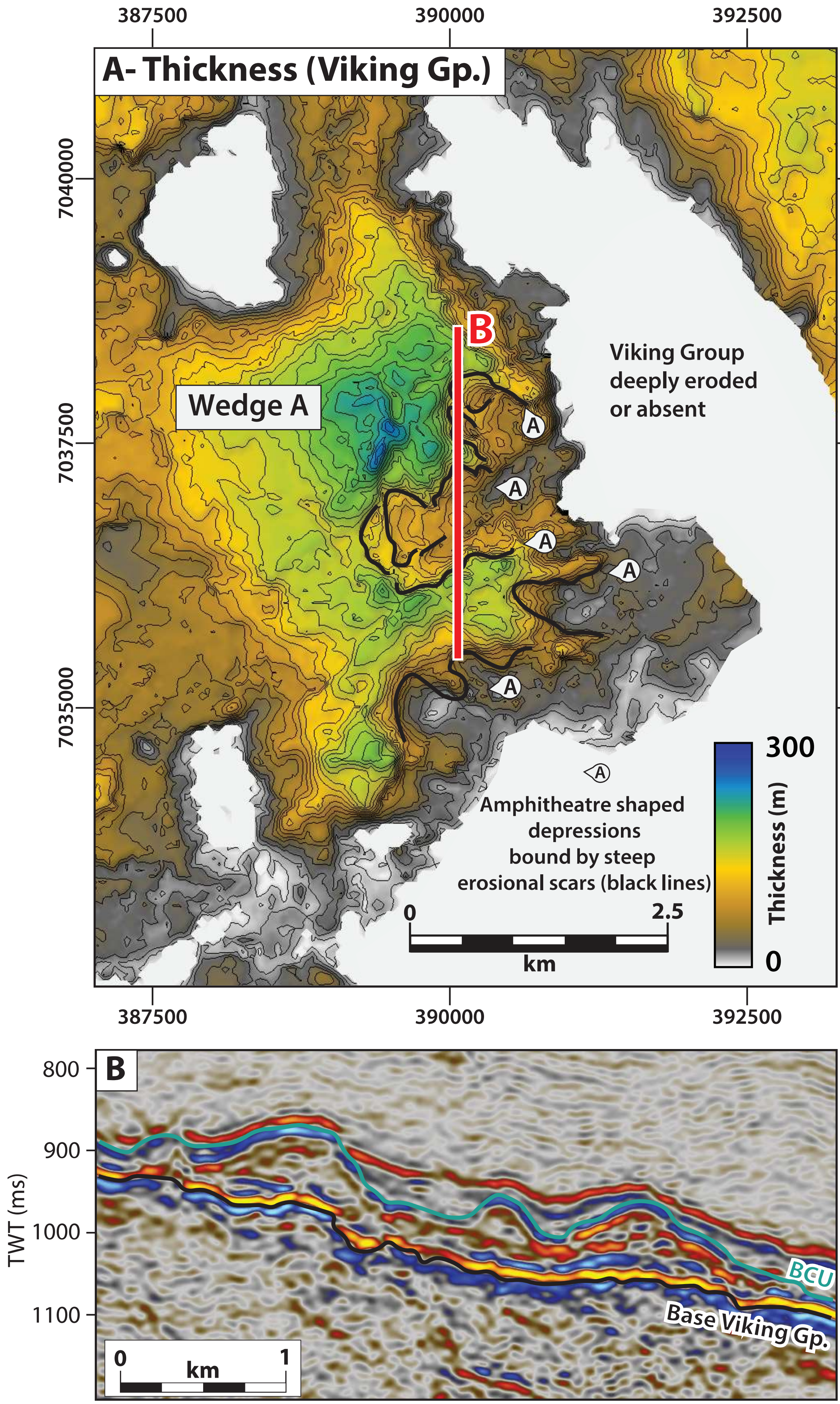

387500
390000
392500
7040000
7037500
7035000
A- Thickness (Viking Gp.)
B
Wedge A
A
Viking Group
deeply eroded
or absent
Amphitheatre shaped
depressions
bound by steep
erosional scars (black lines)
0
2.5
km
300
0
Thickness (m)
B
800
900
1000
1100
TWT (ms)
BCU
Base Viking Gp.
0
km
1

FIGURE 11

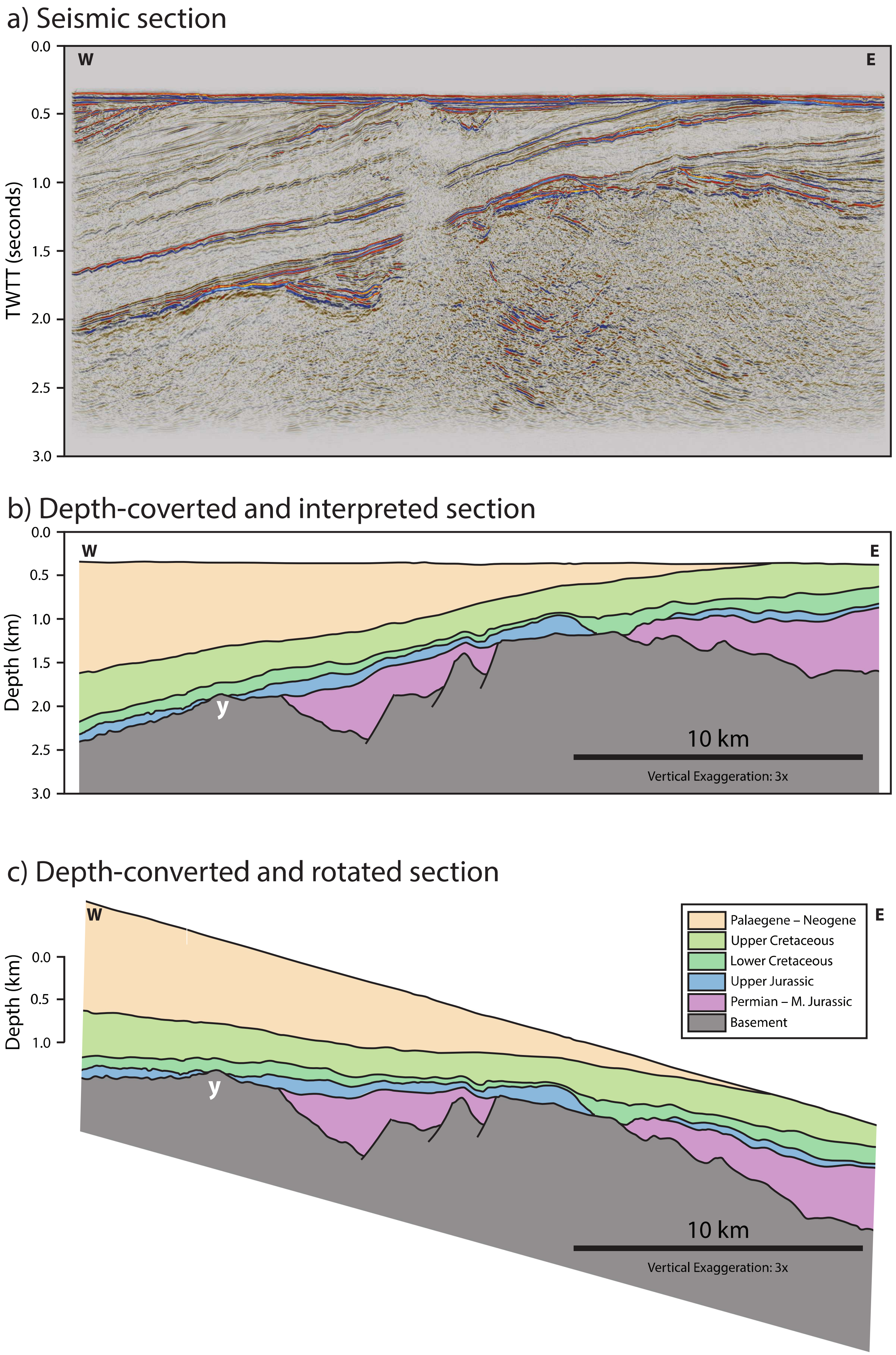
a) Seismic section
W
E
TWTT (seconds)
0.0
0.5
1.0
1.5
2.0
2.5
3.0
b) Depth-coverted and interpreted section
W
E
Depth (km)
0.0
0.5
1.0
1.5
2.0
2.5
3.0
y
10 km
Vertical Exaggeration: 3x
c) Depth-converted and rotated section
W
E
Depth (km)
0.0
0.5
1.0
y
Palaegene – Neogene
Upper Cretaceous
Lower Cretaceous
Upper Jurassic
Permian – M. Jurassic
Basement
10 km
Vertical Exaggeration: 3x

FIGURE 12

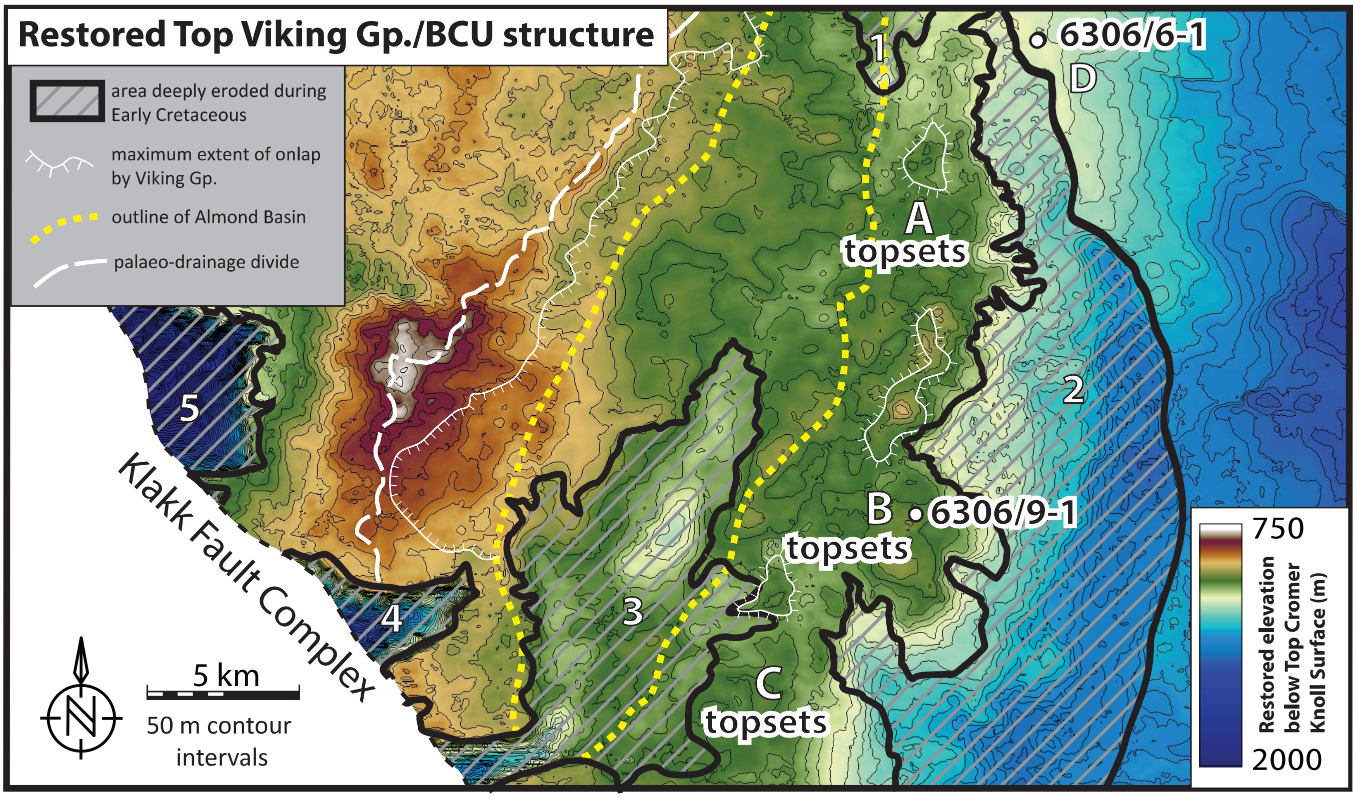

Restored Top Viking Gp./BCU structure
area deeply eroded during Early Cretaceous
maximum extent of onlap by Viking Gp.
outline of Almond Basin
palaeo-drainage divide
1
6306/6-1
D
A
topsets
2
5
Klakk Fault Complex
B
6306/9-1
topsets
3
4
C
topsets
5 km
50 m contour intervals
750
Restored elevation below Top Cromer Knoll Surface (m)
2000

FIGURE 13

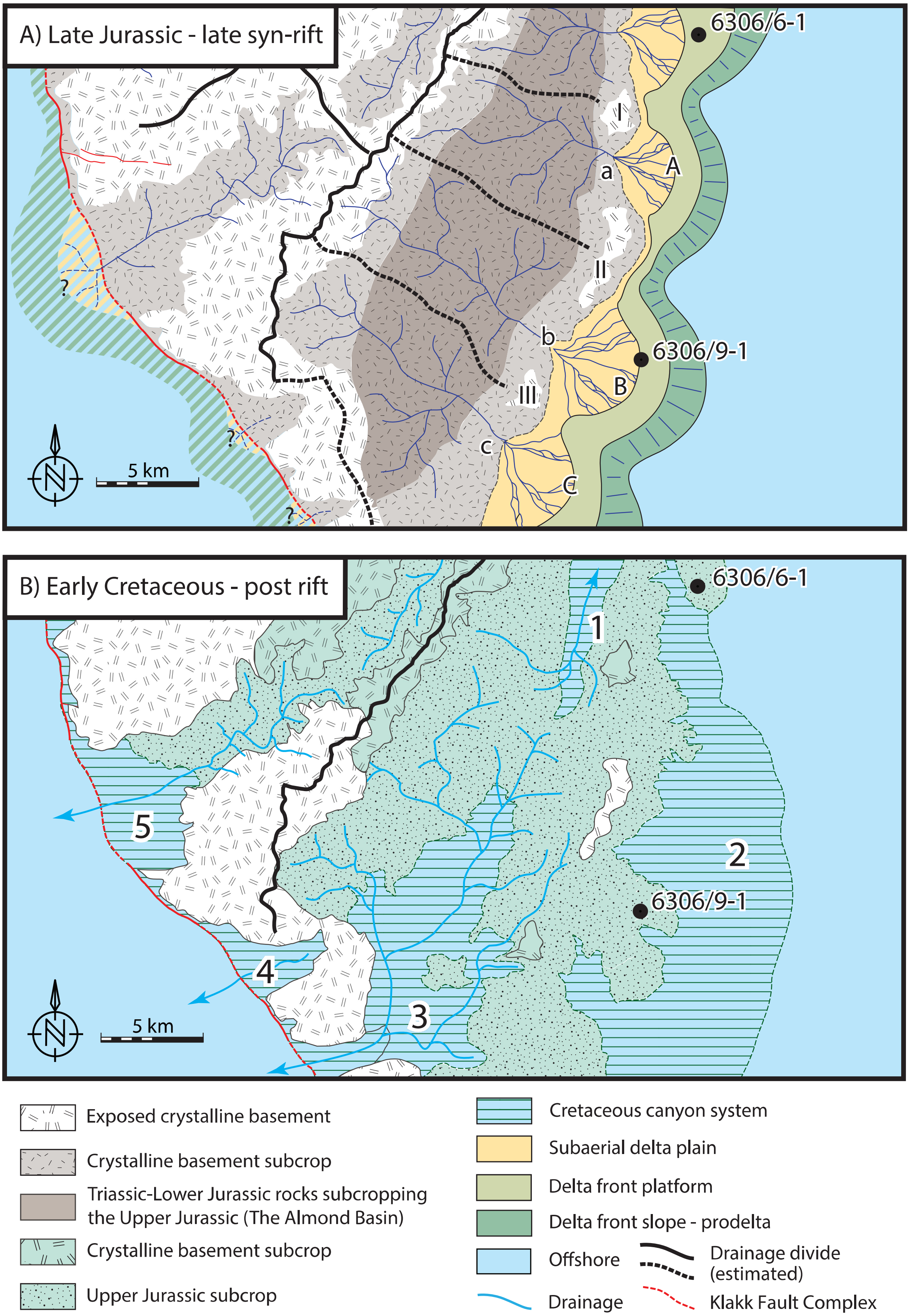

A) Late Jurassic - late syn-rift
6306/6-1
6306/9-1
I
II
III
a
b
c
A
B
C
?
5 km
N
B) Early Cretaceous - post rift
6306/6-1
6306/9-1
1
2
3
4
5
5 km
N
Exposed crystalline basement
Crystalline basement subcrop
Triassic-Lower Jurassic rocks subcropping the Upper Jurassic (The Almond Basin)
Crystalline basement subcrop
Upper Jurassic subcrop
Cretaceous canyon system
Subaerial delta plain
Delta front platform
Delta front slope - prodelta
Offshore
Drainage divide (estimated)
Drainage
Klakk Fault Complex

Figure 14

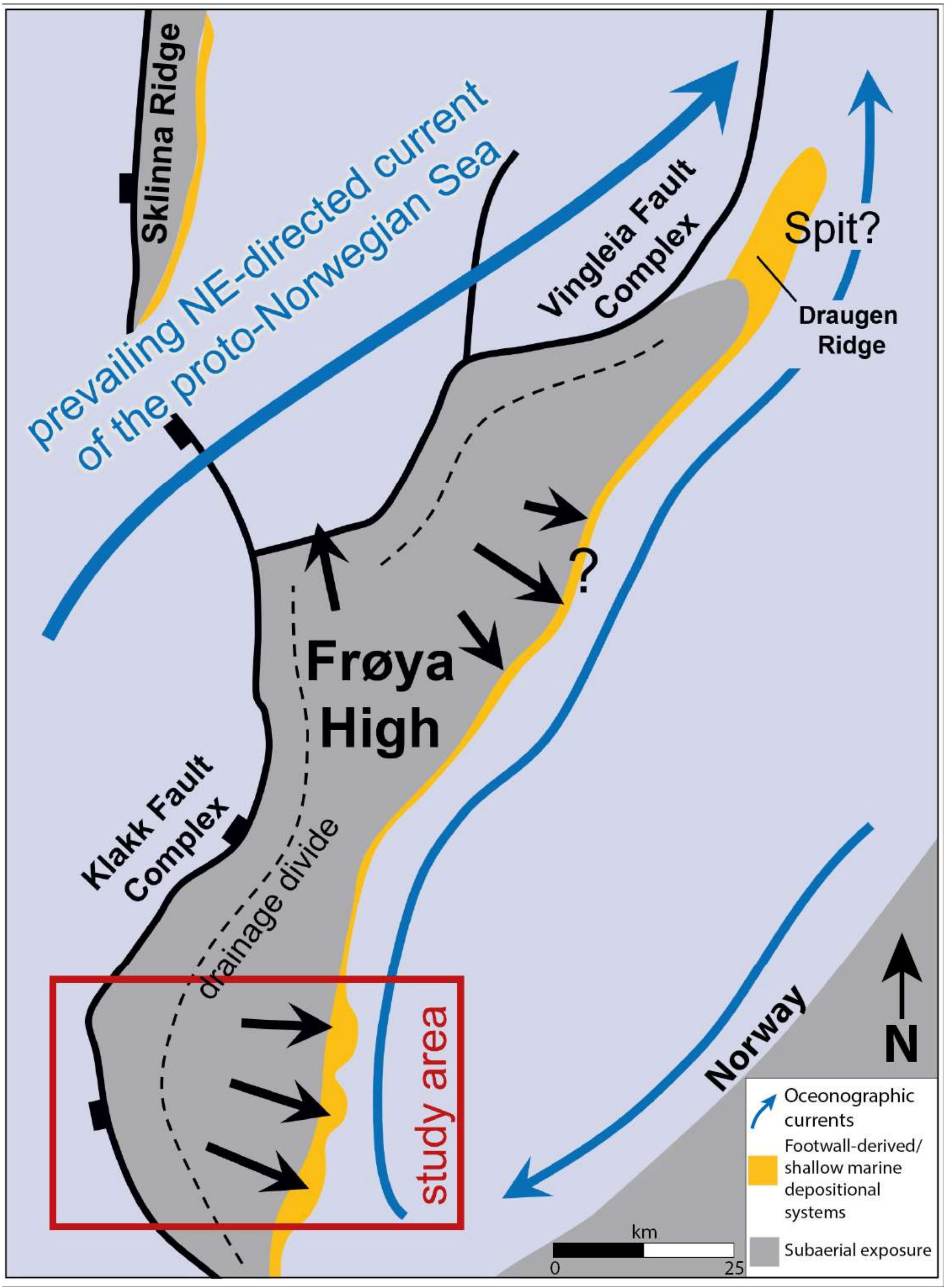

Sklinna Ridge
prevailing NE-directed current
of the proto-Norwegian Sea
Vingleia Fault
Complex
Spit?
Draugen
Ridge
?
Frøya
High
Klakk Fault
Complex
drainage divide
study area
Norway
N
Oceonographic currents
Footwall-derived/ shallow marine depositional systems
Subaerial exposure
km
0
25

FIGURE 15

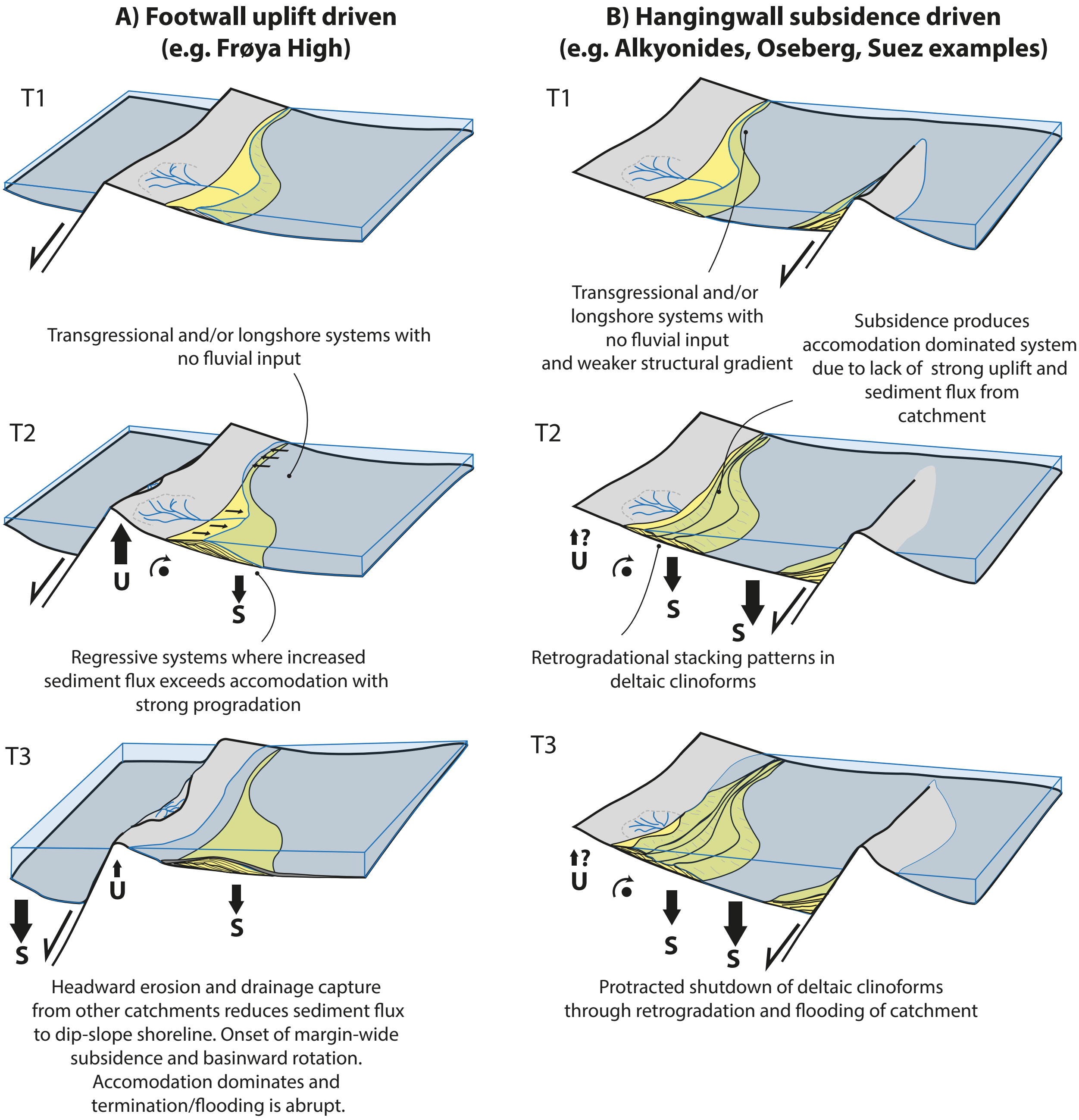
A) Footwall uplift driven
(e.g. Frøya High)
B) Hangingwall subsidence driven
(e.g. Alkyonides, Oseberg, Suez examples)
T1
T1
Transgressional and/or longshore systems with no fluvial input
Transgressional and/or longshore systems with no fluvial input and weaker structural gradient
Subsidence produces accomodation dominated system due to lack of strong uplift and sediment flux from catchment
T2
T2
U
S
↑?
U
S
S
Regressive systems where increased sediment flux exceeds accomodation with strong progradation
Retrogradational stacking patterns in deltaic clinoforms
T3
T3
U
S
S
↑?
U
S
S
Headward erosion and drainage capture from other catchments reduces sediment flux to dip-slope shoreline. Onset of margin-wide subsidence and basinward rotation. Accomodation dominates and termination/flooding is abrupt.
Protracted shutdown of deltaic clinoforms through retrogradation and flooding of catchment